

Review

3-D Metamaterials: Trends on Applied Designs, Computational Methods and Fabrication Techniques

Antonio Alex-Amor ^{1,*}, Ángel Palomares-Caballero ² and Carlos Molero ²

¹ Information Technology Department, Universidad CEU San Pablo, 28668 Madrid, Spain

² Department of Signal Theory, Telematics and Communications, University of Granada, 18071 Granada, Spain; angelpc@ugr.es (Á.P.-C.); cmoleroj@ugr.es (C.M.)

* Correspondence: antonio.alexamor@ceu.es

Abstract: Metamaterials are artificially engineered devices that go beyond the properties of conventional materials in nature. Metamaterials allow for the creation of negative refractive indexes; light trapping with epsilon-near-zero compounds; bandgap selection; superconductivity phenomena; non-Hermitian responses; and more generally, manipulation of the propagation of electromagnetic and acoustic waves. In the past, low computational resources and the lack of proper manufacturing techniques have limited attention towards 1-D and 2-D metamaterials. However, the true potential of metamaterials is ultimately reached in 3-D configurations, when the degrees of freedom associated with the propagating direction are fully exploited in design. This is expected to lead to a new era in the field of metamaterials, from which future high-speed and low-latency communication networks can benefit. Here, a comprehensive overview of the past, present, and future trends related to 3-D metamaterial devices is presented, focusing on efficient computational methods, innovative designs, and functional manufacturing techniques.

Keywords: 3-D; metamaterials; antennas; design; fabrication techniques; numerical methods; microwave; photonics

Citation: Alex-Amor, A.; Palomares-Caballero, Á.; Molero, C. 3-D Metamaterials: Trends on Applied Designs, Computational Methods and Fabrication Techniques. *Electronics* **2022**, *11*, 0.

Received: 2022-01-31
Accepted: 2022-01-31
Published: 10.3390/electronics11030410

Publisher's Note: MDPI stays neutral with regard to jurisdictional claims in published maps and institutional affiliations.

Copyright: © 2022 by the authors. Licensee MDPI, Basel, Switzerland. This article is an open access article distributed under the terms and conditions of the Creative Commons Attribution (CC BY) license (<https://creativecommons.org/licenses/by/4.0/>).

1. Introduction

The appearance of metamaterials has supposed one of the biggest revolutions in the field of electromagnetics in this century [1]. Metamaterials are human-made composite structures that allow for tailoring the propagation of electromagnetic and acoustic waves in media. These artificial structures go beyond the properties of their constitutive materials; namely, the geometrical disposal of their elements (frequently named “meta-atoms”) determines to a great extent their mechanical or electrical response, similar to crystals and protein chains. The most outstanding point about metamaterials is that they can be engineered to exhibit unusual properties rarely found in nature [2,3], i.e., artificial magnetism (magnetism without inherent magnetic materials), negative-refractive indexes from positive-index materials, invisibility cloaking (“invisible” materials that do not interact with light), non-reciprocal phenomena, and chiral responses, such as the one schematized in Figure 1.

Up until now, communities of scientists and engineers have put their efforts into one-dimensional (1-D) and two-dimensional (2-D) metamaterials [4,5], leaving three-dimensional (3-D) configurations to the side. The reason for this is the high design complexity involved in 3-D metamaterials compared to its 1-D and 2-D counterparts. Nonetheless, the increased complexity is worth the price to pay.

arXiv:2112.13750v2 [physics.optics] 31 Jan 2022

Three-dimensional metamaterials present advantages compared with one- and two-dimensional metasurfaces [6]. In general, these advantages are attributed to the fact that a 3-D structure allows the degrees of freedom in both the transversal and longitudinal directions to be exploited in design. In other words, there are more geometrical parameters to tune the behavior of the device. Thus, 3-D metamaterials lead to *advanced functionalities* that are difficult to achieve with 1-D and 2-D configurations, from which future communication systems and smart radio environments can benefit [7]. An example of advanced functionality is the independent control of two orthogonal polarization states, which permits the same structure to act simultaneously as a beam scanner (splitter/steerer) and wave absorber [8]. Moreover, the efficiency can be improved in 3-D structures by avoiding the use of dielectric materials and by directly considering fully metallic implementations [9]. This is not possible in planar structures manufactured with traditional printed circuit board (PCB) techniques, where the metasurface is attached to a dielectric substrate. In addition, 3-D structures can be easily scaled to other frequency ranges as long as fully metallic designs are considered.

Naturally, these advantages come at a price. Three-dimensional metamaterials are bulkier than planar structures, and for some purposes, this can be prohibitive. They also demand greater computational resources and are significantly more complex to manufacture, which have limited their implementation in the past. This trend has changed in recent years, thanks to the massive technological progress in computer electronics (increased computational power) and the development of 3-D printing techniques. This can be appreciated in Figure 2, where metamaterials of different fields (mechanics, acoustics, and electromagnetics) are illustrated.

In this paper, we present an overview of the most outstanding recent developments related to 3-D metamaterials. The document is organized according to the following contents. In Section 2, a review of the most relevant computational techniques applied to 3-D metamaterials is presented. In Section 3, we discuss on some relevant works that have exploited the advantages of 3-D metastructures for the design of functional electromagnetic devices. In Section 4, we review the fundamental fabrication techniques for 3-D prototyping. In Section 5, we discuss on some future challenges and promising approaches related to 3-D design. Finally, conclusions are drawn in Section 6.

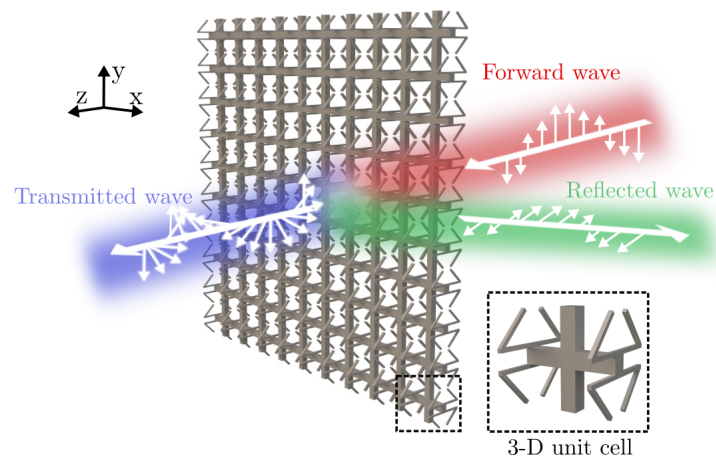


Figure 1. A conceptual illustration of a 3-D metamaterial controlling the flow of light.

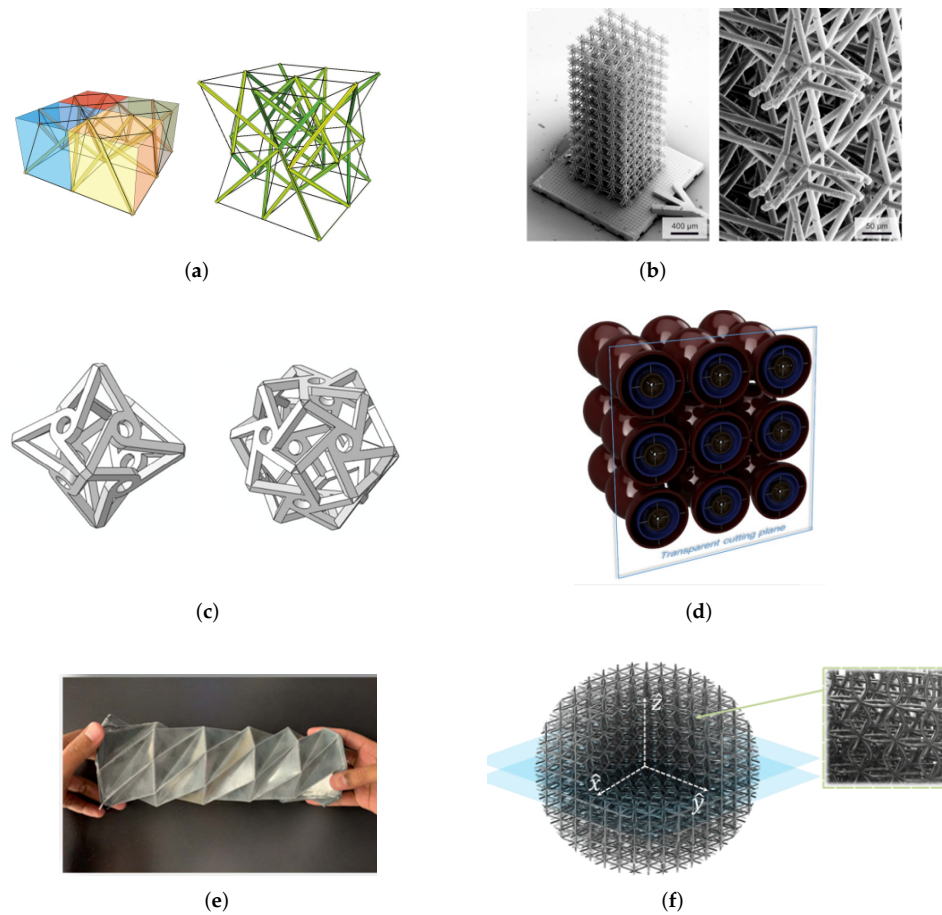


Figure 2. Examples of 3-D metamaterials. (a–c) Mechanical metamaterials [10–12]. (d) Acoustic metamaterial [13]. (e) Antenna [14]. (f) Electromagnetic metamaterial [15].

2. Computational Methods

In a world where mass device prototyping takes a long period of time and costs thousands or million dollars, computational methods are fundamental to predicting the electromagnetic behavior of devices and, therefore, to reduce costs in manufacturing. Regrettably, there is no perfect method that meets all of the simulation requirements (accuracy, fast computation, robustness, flexibility, etc.) and adapts to all scenarios in an efficient manner. Each method possesses *strengths and weaknesses* that make it appropriate for specific domains and unsuitable for others [16]. Thus, it is a common situation to find hybrids of different methods to improve computation efficiency. This section reviews the most relevant computational electromagnetic methods for 3-D structure design and highlights the domain of interest where these methods can be smartly applied.

2.1. Differential-Form Methods

Maxwell's equations can be understood in either integral or differential forms [17]. The latter seeks to represent electromagnetic field propagation as a set of differential equations. Logically, analytical solutions can only be found in very restricted and simple scenarios. Thus, numerical approaches are required to give approximate solutions to the configurations under study. Numerical solutions based on differential-form methods are often referred to as full-

wave approaches, with the two most popular tools being the finite difference method and the finite element method.

The simplest full-wave technique used to solve the complete set of Maxwell's equations is the *finite difference method* [18,19]. The original work developed by Yee in 1966 [20] sought to transform the original Maxwell's equations into difference equations to solve a variety of 3-D electromagnetic problems. This would be a finite-difference time-domain (FDTD) scheme. Nonetheless, finite differences can be directly applied in the frequency domain when time-harmonic fields are considered. This would be a finite-difference frequency-domain (FDFD) scheme [21]. Comparing both, FDTD is normally preferable to analyze transient and nonlinear phenomena while FDFD is a better option for electrically large structures. As an example, FDTD schemes are implemented in [22–24] for the analysis of 3-D (nano) cavities and woodpile structures, respectively. FDFD techniques have also been implemented to model the scattering phenomena in isotropic [25] and anisotropic [26] 3-D objects, and the dispersion properties of open nanophotonic resonators [27].

One of the most widely implemented technique in commercial packages is the *finite element method* (FEM). This is essentially due to its facility to deal with non-trivial scenarios in a more efficient way than a traditional finite difference scheme in exchange for a greater complexity in its mathematical implementation [28]. Similar to FDTD and FDFD, the whole space in FEM is discretized into small pieces, in this case, called finite elements. In a Galerkin approach of the FEM, the residual of the so-called weak form is forced to be orthogonal to some predefined test functions and the fields are expanded as a set of basic functions. This leads to a finite system of linear equations that can be solved with direct or iterative methods. Some examples of in-house FEM formulations applied to electromagnetic 3-D design can be found in the literature. In [29], a FEM was developed for the design of efficient cloaks applied to spheroidal metallo-dielectric objects. Another example can be found in [30], where a FEM was applied to compute EM fields in 3-D nano-photonic crystals and waveguides. However, as the FEM is such a generalist method, the common scenario is to perform FEM computations through commercial simulators as CST, COMSOL, or Ansys HFSS. This is the case in [31], where the proposed analytical model for chiral 3-D elastic metamaterials is checked with FEM calculations performed with commercial simulator COMSOL Multiphysics [32].

2.2. Integral-Equation Methods

Different from finite difference and FEM schemes, integral-equation methods incorporate radiation conditions in a natural form, so there is no need to include absorbing boundary conditions to restrict the simulation domain [33]. In addition, integral equations allow for a reduction in the dimension of the problem by one by only setting unknowns on the boundaries instead of discretizing the entire volume [34]. These motives have propelled the use of integral-equation methods in branches of electromagnetism such as antenna theory or microwave circuits [35].

The most famous integral-equation method is known as the *method of moments* (MoM), occasionally named the boundary element method in other fields of physics [36]. In the MoM, the unknown function f to be determined is expanded inside the integral as a set of known basis functions b_k with unknown coefficients a_k ; namely, $f(\mathbf{r}, t) \approx \sum_k a_k b_k(\mathbf{r}, t)$. This eventually leads to a linear system of equations with unknown coefficients a_k that can be solved after considering the appropriate boundary conditions. MoM has been traditionally applied in the study of wire and planar antennas [36–38] as well as in single-layer reflectarray/transmitarray configurations [39]. These works were then extended to include planar multilayered (2.5-D) devices [40–43]. However, it is not so common to find actual 3-D implementations with the MoM, which is a difference from full-wave numerical methods. This is mainly due to the greater difficulty in defining proper basis functions for complex 3-D geometries and to the

substantial increase in time complexity compared with 1-D and 2-D structures. Nonetheless, some interesting examples can be found in the literature. For instance, MoM formulations are developed in [44] (combined with a plane-wave expansion) for an analysis of 3-D metallic wire media and in [45] to compute the eigenstates of periodic metamaterials, with application to 3-D arrays of spheres.

Nyström method is an alternative to method of moments. In the Nyström (quadrature) method, integrals are directly replaced by weighted sums [46]. It is generally more computationally costly compared with MoM but can also offer more accurate results as higher-order quadrature rules can be easily implemented. The Nyström method is particularly convenient compared with MoM when a mixture of several media of different characteristics has to be considered in the computation. An example of its use applied to the study of scattering phenomena in 3-D objects and composite structures can be found in [47,48].

The *fast multipole method* (FMM) is an integral-equation method extensively used for the resolution of gravitational and electromagnetic problems [49]. The essential idea behind the FMM is to locally approximate a simple radiating point by superposing a finite number of plane/spherical waves in the direction of propagation; namely, expanding the system Green's function using multipole series terms. Different aspects related to the numerical implementation are extensively detailed in [50]. Since the FMM is a quite efficient computational technique to perform matrix–vector products, it is commonly found in combination with basic MoM methods to speed up the resolution of the linear system. An example can be found in [51], where a hybrid FMM–MoM method is employed to analyze the scattering of electromagnetic waves in 3-D nanoparticle systems.

The *Wiener–Hopf method* is a powerful technique for solving certain types of integral equations. By making use of the Laplace transform (Z transform in discrete implementations), it is possible to transform the original expression into a functional equation that is suitably defined in the complex space [52]. In the context of electromagnetics, its use is convenient in periodic problems, where the periodicity is considered a space sampling. Concretely, the Wiener–Hopf method has proven to be particularly insightful and efficient in truncated periodic configurations, such as the semi-infinite 3-D plasmonic media presented in [53]. Thanks to the use of this method, edge diffraction terms and bound surface waves launched by the edge condition (terms that are not excited in infinite structures) have been clearly identified [54].

Worthy of special mention is *Ewald's method*, traditionally used for the efficient computation of free-space periodic Green's functions [55]. The underlying idea of Ewald's summation method is to rewrite a generic periodic Green's function as a sum of two quickly-convergent series: the first sum (actual space) exponentially decreases by itself, and the second sum (Fourier-reciprocal space) quickly decays for large arguments. Ewald's method has been typically applied to compute the dispersion properties in 3-D periodic arrays of electric and magnetic dipoles [56,57] and in 3-D skewed lattices [58].

2.3. Modal Analysis

In modal analysis techniques, the fields are expanded as a series of orthogonal eigenfunctions weighted by complex coefficients. The amplitude of these coefficients are fixed by the boundary conditions and the geometry of the considered object. As a difference with purely numerical approaches, modal techniques are direct and bring physical insight to wave propagation and scattering phenomena while maintaining fast computation times [59].

Modal techniques are normally applied in closed structures where the fields are confined, such as waveguides and coaxial lines [60]. In fact, the analysis of waveguide junctions and discontinuities is one of the most characteristic applications of modal analysis, which raised a lot of interest in the engineering community for the design of filters, diplexers, orthomode transducers, and other interesting microwave devices. This is performed by imposing the

continuity conditions of the tangential fields in a process that is normally referred to as *mode matching* (MM) [61].

In addition, modal techniques are also intensively applied for the analysis and design of metamaterials. Plane waves are solutions to Helmholtz wave equation and form a proper basis to represent EM fields in periodic structures [62]. *Plane-wave expansions* (also known as Floquet–Bloch expansions) are modal representations of the fields in the region of interest. Thanks to the Floquet–Bloch theorem, the whole computation domain can be reduced to a single unit cell in periodic configurations and, therefore, the plane-wave expansion, notably reducing the computational requirements of the simulation.

Multiple examples of modal expansions applied to metamaterials and antennas can be found in the literature. In [63,64], a modal analysis was carried out to compute the dispersion properties of 3-D periodic arrangements of spheres, with potential application to complex nanoparticle systems. A MM technique was formulated in [65] for the analysis of bi-periodic cylindrical structures and wire media. In [66], a hybrid MM-FDFD was developed for the analysis of electromagnetic bandgap (EBG) structures and substrate-integrated-waveguide (SIW) antennas. In [67], dual-polarized fully metallic metagratings constituted by short-circuited periodic waveguides were analyzed with a MM technique. Periodic arrays of helical structures forming chiral metamaterials were studied in [68] by means of modal analysis techniques. In addition, efficient semi-analytical formulations based on the mode-matching method and Floquet modal expansions were developed recently for the analysis of metasurfaces and transmission lines involving higher symmetries (glide and twist) [69–72]. These formulations have potential to be adapted to mimic the interesting properties associated to higher symmetries (low dispersion, wideband, and higher refractive index) in more complex 3-D structures.

2.4. Circuit Models

Circuit models are insightful tools that allow for a simple representation of the underlying physical reality. Interestingly, they are noticeably more computationally efficient compared with the aforementioned methods, most of the time, at the cost of a lower accuracy in the computation. These features make circuit models a suitable option for the modeling of microwave devices, frequency selective surfaces, and metamaterials [73–75].

There are different methods to obtain a *circuit model* in periodic configurations: (i) heuristic rationale, namely, simple circuits based on experimental knowledge (capacitive/inductive coupling, losses modeled as resistances, etc.) that provide physical insight but work for very particular structures, usually in a limited frequency range [76,77]; (ii) synthesis methods, that is, more rigorous (and complex) formulations that give accurate results but require prior full-wave simulations [78–80]; and (iii) analytical methods, namely, rigorous circuit approaches, based on Floquet modal expansions [81–83] or first-principle computations (i.e., integral equations) [84, 85], that provide accurate results and are independent from commercial full-wave simulators but are often restricted to canonical geometries.

Recent advances in circuit modeling have considered stacks of periodic 2-D arrays [78,86] and the potentials of these methods are somehow broader than expected [87]. Nonetheless, stacks of 2-D arrays do not really exploit the design the degrees of freedom associated with the longitudinal (propagating) direction. For this reason, they are often referred to as 2.5-D structures. In fact, there is still a lack of studies in the literature on general circuit approaches that can model 3-D configurations. Only a few selected examples can be found. In [88], the proposed isotropic 3-D negative-refractive-index medium was modeled by means of a circuit model consisting in transmission lines loaded with reactive elements. In [89,90], a circuit model based on the transmission-line matrix scheme (TLM, see [91]) was proposed for 3-D composite right-left-handed isotropic metamaterials.

The design of 3-D square waveguide cells for implementing full-metal devices was recently investigated by the authors. In [92], a quasi-analytical circuit approach that combines analysis and synthesis procedures was developed for the design of full-metal polarizers. In [93], a periodic 3-D metamaterial formed by laterally perforated square waveguides that exploit phase resonances was analyzed by means of a heuristic circuit approach. Finally, a heuristic circuit (assisted by full-wave computations in commercial software CST) was presented in [94] for the simplified design of complex broadband 3D-printed polarizers based on electro-magnetic elements.

2.5. Other Methods

Although the most popular and generalist methods have already been discussed, there are many other solutions that are particularly efficient when applied to some particular configurations and structures. This would be the case of the homogenization, ray-tracing, and transfer-matrix methods.

Homogenization theory seeks to model the electromagnetic behavior of complex media through their effective (average) constitutive parameters. Homogenization methods based on first-principle computations and the use of integral equations have been particularly useful for the analysis of 3-D wire media [95–98], epsilon-near-zero materials [99], 3-D resonators [100], and 3-D non-magnetic configurations [101]. A different example of homogenization model can be found in [102], where the effective parameters of a glide-symmetric metamaterial were derived with a mode-matching formulation.

Ray theory describes light propagation and, more generally, wave propagation in terms of rays, a geometrical simplification to represent light paths [103]. Ray-tracing methods are efficient tools used to estimate propagation features in very large domains and multi-scale problems, where FEM or finite difference methods require huge computational resources. In contrast, ray theory is valid as long as the wavelength is small compared with the dimensions of the considered objects. In electromagnetics, ray-tracing techniques have been intensively applied for the study of optical and microwave lenses, fiber optics, as well as reflectarray cells [8,104–106]. Moreover, ray tracing is extensively used for channel categorization in wireless communications, i.e., to estimate channel features of 5G networks [107,108].

The *transfer-matrix method* is a numerical tool for the computation of band structures (phase and attenuation constants) in periodic configurations. This method relies on the extraction of the so-called transfer matrix, which defines the properties of a single unit cell, and the subsequent resolution of an eigenvalue problem [109]. This method has proven to be valuable in many configurations, even in those involving complex metamaterials embedded in anisotropic media [110]. In order to extract the transfer matrix, different approaches can be used. Some works take advantage of general-purpose commercial software to extract the transfer (or scattering) matrix. This would be the case of [111], where a 3-D configuration consisting in a corrugated dielectric waveguide with absorbing layers is analyzed. Similarly, a double wire-mesh structure that suppresses the cut-off frequency is analyzed in [112]. Other works implement in-house techniques to extract the transfer matrix. This is the case exposed in [113], where a transfer-matrix method based on a plane-wave expansion is developed for the computation 3-D photonic platforms (i.e., a woodpile structure).

Table 1 presents a summary of the main features related to all discussed computational techniques. The strengths of each method are marked in bold type.

Table 1. Strengths and weaknesses of the discussed computational techniques applied to 3-D design. Legend: “L” states for low, “M” states for medium, and “H” states for high.

Methods	Generality, Robustness	Mathematical Complexity	Computational Complexity	Accuracy	Physical Insight
Finite Differences	M-H	M	M-H	M-H	L
Finite Elements	H	H	H	H	L
Integral Equations	M-H	M-H	M-H	M-H	M
Modal Analysis	M	M-H	M	M-H	M-H
Circuits	L-M	L-M	L	L-M	H
Ray Optics	L-M	L-M	L-M	L-M	M-H
Homogenization	L-M	L-H	L-M	L-M	M-H
Transfer Matrix	M	L-M	M	M	M

2.6. Commercial Solvers

Commercial simulators are robust general-purpose tools employed for the resolution of a multitude of engineering and physics problems. Their development has been enormous, and these days it is normal to find them embedded in a complete suite that includes many types of solvers that adapt to the simulation requirements: frequency/time domain, large/finer mesh, etc. These solvers are normally based in the methods previously discussed in this section.

In the field of electromagnetics, three of the most popular commercial simulators are CST Microwave Studio [114], Ansys HFSS [115], and COMSOL Multiphysics [32]. CST and HFSS share some similarities in their internal design. Both have a complete suite of solvers. In CST, the frequency-domain solver employs a FEM method, the time-domain solver employs a finite integration technique (a generalization of the FDTD method), the integral-equation solver combines a standard MoM with a fast multipole method (FMM), and a ray-tracing solver is available for very large structures. Similarly, the frequency-domain, integral-equation, and ray-tracing solvers in HFSS employ FEM, MoM, and ray-theory methods, while the time-domain solver is based in a FEM in this case. On the other hand, COMSOL Multiphysics is primarily based on FEM formulations that make use of either direct (LU decomposition) or iterative solvers.

3. Designs

A large number of functionalities can be attributed to 3-D metamaterials, as can corroborated in the literature (mainly papers from the current century). It can be established that the beginning of metamaterials was linked to the experimental verification of negative permittivity and permeability in artificial materials [116]. The primary prototype of a metamaterial consisted of a 3-D periodic distribution of split-ring resonators, performing electrical properties not accessible in nature and *easily* tunable. Many researchers paid attention to these exotic properties, giving rise to the development of potential applications, such as those in the field of magnetic resonances [117,118]. The 3-D architecture of split-ring prototypes is otherwise difficult to model. It is worth remarking the homogenization technique reported in [119], reducing the analysis of such a complicated architecture to simple equivalent circuits. As mentioned in the previous section, homogenization techniques are well known and have encouraged the study of some other types of complicated 3-D structures [96,120]. Such is the case of artificial photonics crystals, reported by Dr. Sievenpiper et al. before the metamaterials *boom* [121]. Artificial photonic crystals were motivated by the well-known propagating properties of photonic

crystals, emulated, for example, in metasurfaces operating in the THz regime [122], specifically wire mesh photonics crystals formed by fully metallic lattices of parallel rods [123] or interconnected wires under exotic geometries [124–126]. The interest in these topologies especially lies in the inherent propagation properties, leading to anisotropy and effective-permittivity control [127,128]. Applications straightforwardly profiting these properties involve near-zero permittivity materials, directivity enhancement, or subwavelength imaging.

Successive evolutions and extensions of wire metamaterials have emerged and have been reported in the last decade. Three-dimensional designs based on cells including non-connected helical wires are noteworthy in exploiting chirality, such as the one in [129] or that in [130]. The latter considered helical elements with exotic orientations and combinations in order to enhance the chiral properties. Chirality is a powerful tool providing polarization manipulation in the form of linear-to-circular conversion [129,131] or linear-to-linear field rotation [131,132]. The physical mechanism behind the field conversion profits from the inherent anisotropy of chiral elements, which manipulates the co- and cross-polar field components when the whole structure is fed by an impinging plane wave. A quite interesting study of chirality regarding a set of cell candidates was reported in [133]. Additional prototypes based on periodic distributions of connected and non-connected wires have also been studied and reported for different purposes. Such is the case in [134], where a narrow-band three-dimensional lens was constructed, or the cases in [135,136] reporting periodic distributions of folded-wires with the aim of enhancing angular stability. It is finally worth remarking the very original designs conceived by the group of Prof. Mittra in the last decade, turning the screw of the geometry in wire metamaterials [137–139]. The unit cell comprises two metallic Jerusalem crosses separated by a certain distance and connected via bifilar lines. This configuration is fed by external plane waves, exhibiting wideband response with angular robustness.

An alternative and very important family of 3-D periodic structures has mainly been developed by Prof. Shen and his research group. Their designs can easily be recognized by a particular physical architecture, and their optimization techniques are based on well-constructed multi-modal mathematical approaches. A first review was published in 2014 in [140]. The interest in these architectures lies in the large number of functionalities that can be invoked thanks to, among other reasons, the introduction of resonators extended along the propagation direction. The orientation of the resonators breaks up the axial symmetry typical from 2-D periodic arrays, adding new degrees of freedom (geometrical parameters) to the structures.

As can be checked in their papers, the general prototype proposed by them are two-dimensional periodic arrays formed by unit cells emulating a sort of microstrip geometry. See, for example, [141] or [142], where cells with similar appearance are used for different functionalities. In particular, the cells in [141,143] are employed to exhibit bandstop operation. This physical mechanism behind bandstop response is mainly governed by strip and dog-bone-shaped resonators included along the microstrip and is better understandable thanks to the derivation of equivalent circuits. The use of circuits was also necessary to invoke the inverse operation (bandpass) in the original cell reported in [144], intended to be used for radome applications. It is worth remarking the complexity encountered to optimize 3-D designs in transmission operation. The cell presented in [145] is an example, where stepped-slits along the axial direction govern the transmission properties of the whole device, but only single-pol operation is possible. A similar configuration having dual-pol operation is presented in [146], providing a circular polarizer for the Ku-band.

The *pseudo*-microstrip geometry has otherwise been highly exploited for applications involving radar cross-section reduction, low observability, and multi-channel selection. This is possible thanks to the efficient combination between the inherent wideband and multiband nature of the cell with resistive elements. The most straightforward design was presented

in [142] after combining the cell-type in [141] with commercial resistors. The result was a dual-pol wideband absorber experimentally tested with success. Other variants of wideband absorbers were reported in [147,148], where the unit cell comprises long folded strips. Multi-path cells constitute a third variant of absorbers, in which the operation band is controlled by resistive pin-diodes [149]. Ultrawideband absorbers can also be used to design absorptive frequency-selective transmission (AFST) [150,151] or frequency-selective reflection structures (AFSR) [152,153]. The latter are better known as *rasorbers*. The main property of both models is the characteristic spectral response, which introduces a transmission/reflection band in the middle of a wide absorption band. In other words, the devices are configured to transmit/reflect incoming waves of which the frequency is inside a particular band and discriminate (absorb) incoming waves with the rest of frequencies. Unit cells with multi-path configurations based on exotic designs of microstrips are again employed. Specifically, the strategy consists of designing cells having artificial and parallel paths (transmission lines connected in series), where some of them are *resistive* pathways for the traveling waves and the rest stay lossless [154, 155]. This combination, when properly optimized, introduces sequences or concatenations of transmission/reflection and absorption bands. The resistive pathways can be constructed by the use of magnetic materials [155–157]. They are materials artificially designed to have larger permeability loss tangent. The propagation along them is highly lossy, contributing to an efficient absorption. A visual example of a cell of this kind is sketched in Figure 3a. Other ways to design resistive pathways are the introduction of commercial ferrites [158] or commercial resistors [154,159].

Periodic distributions of waveguide-cell configurations constitute another great family of 3-D structures. Waveguide-cell topologies involve fully metallic, fully dielectric, or metallo-dielectric designs with square cross section. Naturally, they are generally complemented with the introduction of resonators along the axial direction with the aim of profiting from a bigger number of degrees of freedom. It is noteworthy to begin with a first sub-family labeled as *square-coaxial* waveguides [136,160,161]. The cell is formed by concentric dielectric and metallic square rings, all having the same length. The dielectric materials are commonly commercial resins and plastics suitable for 3-D-printing fabrication. This type of cell encourages multi-channel transmission, with each single channels being that enclosed in the region between two adjacent metallic rings. As was aforementioned, multi-paths encourage multi-band response (multi-band filters). In this case, the paths are well isolated from each other, giving rise to highly isolated bands with no mutual interference. Furthermore, strong robustness with the incidence angle was achieved. A second version of coaxial waveguide-cells includes free-space channels. This is the case reported in [162,163]. The free-space channel is actually a square hole in the center of the unit cell. It enhances the generation of transmission poles and zeros, encouraging dual-band transmission that can be easily tuned.

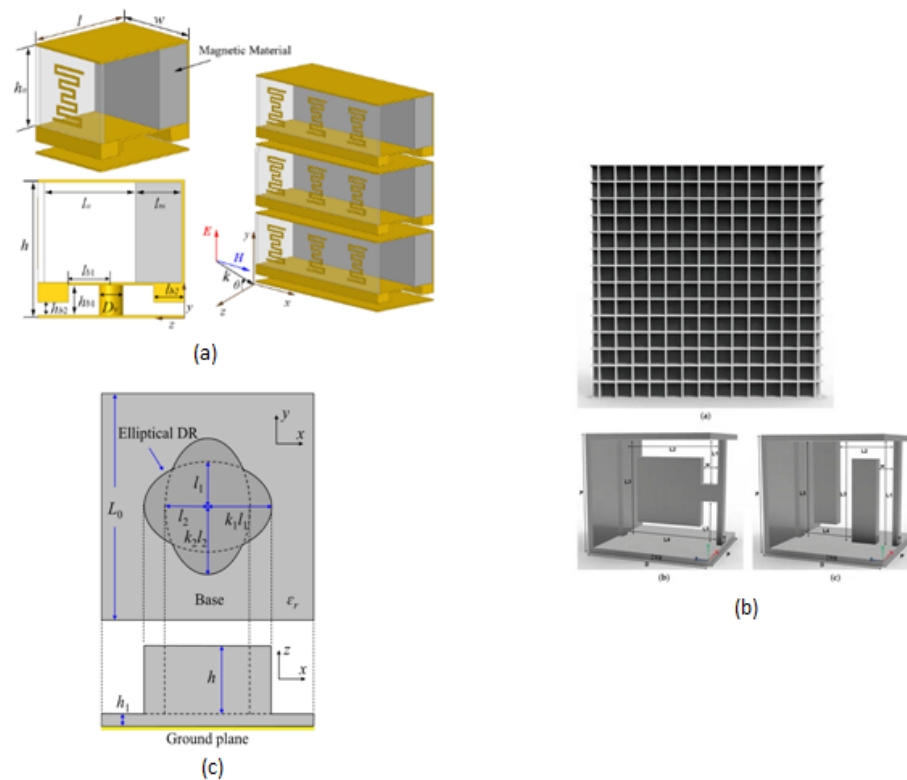


Figure 3. (a): One of the cells conceived for rasorbers. This one was reported in [156]. (b): Full-metal reflectarray prototype reported in [164]. (c): Fully dielectric reflectarray prototype reported in [165].

Full-metal 3-D periodic structures are part of a novel and modern 3-D family. Its development was recent due to the historically high difficulty in achieving mechanically robust and self-supported devices manufactured by metal only. The fast increase in 3-D-printing techniques in recent decade has allowed us to address the fabrication of this type of architectures, though its use is not widespread yet. A massive use is expected in the near future due to future trends and new considerations introduced in recent communications standards, highly keen to cover millimeter bands. Spacial applications are also demanding fully metallic terminals owing to the hard conditions in spacial environments. Dielectric materials are quite limited in these scenarios, from the electromagnetic, mechanical, and thermal point of view. Additionally, dielectric losses become dominant in the far-microwave spectral region and beyond, drastically deteriorating the performance of the devices under use. All of these constraints motivate the search, design, and optimization of 3-D fully-metallic architectures. First attempts have been published in [161] and were later refined in [9,92] with relative success. Fully metallic cells are the basis of the periodic structure, consisting of square waveguides with resonators perforated on the walls. Thanks to the resonators, the control of the transmission features, such as the transmission-band positions and dual-polarization operation, is readily tuned. These properties were successfully synthesized to attain single and dual-pol circular polarizers in [9,92], respectively. The same principles were later applied for the design, optimization, and fabrication of the reflectarray [164] shown in Figure 3b. Furthermore, this same structure is currently the subject of study for a most challenging terminal, which would include reconfiguration with graphene, leading to a metastructure exhibiting several functionalities [8]. The latest version of this structure was recently published [94] and reported slits instead of resonators on the walls. This new architecture is suitable for wideband transmission, since

the TEM mode can be excited in the cell. A wideband circular polarizer has theoretically been predicted and experimentally tested with success.

Finally, we highlight several 3-D prototypes specifically designed and manufactured for a fixed functionality. Such are the cases of 3-D reflectarrays/transmitarrays and 3-D lenses. In both cases, the use of periodic structures is no longer possible due to the need to implement phase gradients all along the surfaces. Since the cell distribution is considered *pseudo* periodic, we use the term *metasurface*. In the last decade, the use of metasurfaces has increased worldwide, thanks to the numerous theoretical predictions that have been corroborated experimentally, and in application fields where they have become essential [166]. Metasurfaces are low-profile terminals constituted by cells in which the spacial dimensions do not overcome the operation wavelength (in contrast with multi-layer versions of 2-D periodic metasurfaces). This makes them highly attractive, especially when terminals with small sizes are required. For instance and as mentioned above, spacial applications demand low-weight, low-profile and fully-metallic devices for future missions. Fully metallic reflectarrays are still challenging, but some prototypes have been launched. This is the case in [164] (previously cited) and in [167]. This latter is quite interesting because the reflectarray was mechanically reconfigured and optimized to operate in the Ka-band. Furthermore, it has a privileged architecture to provide wideband operation in frequency. A fully metallic transmitarray was presented in [168] for the Ka-band, with wideband response and excellent insertion losses. Examples regarding fully dielectric reflectarrays do also exist in the literature. It is worth mentioning that the term fully dielectric is generally not accurate owing to the inclusion of ground planes that forces the fully reflection operation. In this sense, dielectric reflectarrays based on dielectric substrate with protrusions are the most appealing designs. Paradigmatic examples are reported in [165] with elliptical protrusions (see Figure 3c for visual information) [169] with cross-shaped protrusions and [170] with rectangular protrusions. The protrusions are oriented in order to break the symmetry of the cell, with the role of controlling the vertical and horizontal field components in a context of high but not full independent. This kind of reflectarray provide very wideband response in frequency. Another version of a dielectric reflectarray was published in [171], where the protrusion (C-shaped in this case) was not supported on a dielectric panel but on the ground plane directly. The properties are actually similar to the dielectric reflectarrays previously cited. A final version of a reflectarray is that called *Kirigami* [172], where an effective conformal shape just varies the size of cells. In this particular structures, the cells have a sort of hexagonal shape. In the context of 3-D lenses, it is worthy to highlight the prototypes reported in [173,174], consisting of *Luneburg* and *Fresnel* lenses, respectively. The first of them comprises exotic cubic cells to design the lens in the Ku/K-bands, whereas the second one combines air and dielectric slabs as a way to control the phase of each cell for optimization of the lens in the THz domain. Both cases shows high efficiency and very good gain performances.

4. Fabrication Techniques

Due to the 3-D geometry of the unit cells that compose the metamaterial under studied in this review, new manufacturing techniques and assemblies have had to be employed in order to achieve a satisfactory prototyping. In planar conventional fabrication where metasurfaces offered 2-D geometry, the PCB manufacturing achieved adequate prototyping even when metasurfaces were used to form stacks. However, for the case of unit cell fabrication with 3-D geometry, these results are inadequate and, if used, have to be complemented by more complex assembly. With the development of new manufacturing techniques in *3-D printing*, the task of manufacturing metamaterials with 3-D geometry has been alleviated, allowing for their manufacture with less complexity and higher precision. This also means that, with 3-D printing, prototypes can be produced in a single piece without having to divide the structure into different pieces, to manufacture each one separately, and then to assemble them,

which results in a more tedious process and a greater potential source of errors. In this section, a revision of different works in the literature is carried out, which show a prototype of a unit cell with 3-D geometry. Generally speaking, these can be divided into three types of manufacturing: (1) conventional with 3-D assembly, (2) 3-D printing, and (3) alternative techniques.

4.1. Conventional Manufacturing Techniques and 3-D Assembly

The first one to be described is conventional manufacturing with 3-D assembly. As mentioned above, this fabrication technique can be represented by any traditional manufacturing technique such as PCB manufacturing, computer numerical control (CNC), or electrical discharge machining (EDM), which entails a separate fabrication of the parts that conform the prototype and, later, an assembly of these parts in three dimensions. Examples of this kind of prototyping are found in [141,143,146,163]. In all of these studies, the 3-D unit cells have been manufactured with different PCB layers stacked both horizontally and vertically, forming the sides of the unit cells. To assemble these pieces in a simple way, different grooves are implemented to interlock them all together (see Figure 21c from [143]). In addition to this mechanical assembly, most of these designs require the application of conductive glue [163] or solder [143,146] in the assembly areas (grooves) to avoid any electrical discontinuity that could damage the electromagnetic behavior of the manufactured prototype. An alternative for 3-D assembly with PCB layers is the one presented in [138], where the connecting and supporting elements between the two layers are copper wires, which in turn have a beneficial effect on the electromagnetic response. Thanks to the 3-D geometry of the unit cells, lumped elements or homogeneous materials with a given dielectric properties are relatively easy to insert into the unit cells. Some examples in 3-D PCB assembly are shown in [142,147,156] and Figure 3a illustrates a unit cell where magnetic material is included in its structure. In general, due to the current applications, these external elements are lossy such as resistors or magnetic/dielectric materials to design absorbers [147] or rasorbers [142,156]. However, in these last two studies, additional metal structures (for example, conducting planes) had to be fabricated separately to allow for the integration of the lumped elements or the lossy materials. On the other hand, a conventional manufacturing technique EDM has also been employed to achieve an all-metal metamaterial. One of the example that utilizes this manufacturing technique is the prototype presented in [9]. Thanks to the periodic slot geometry along the horizontal and vertical walls of the waveguides that form the unit cells, in this case, there is no need for 3-D assembly and the prototype is in a single piece. As mentioned in this work, CNC has been discarded as it required a more complex assembly process.

4.2. 3-D Printing

The second type of manufacturing described in this section is one that involves 3-D printers. Within this category, a distinction can be made between prototypes that are 3-D printed on *plastic* with subsequent metallization and prototypes that are 3-D printed *directly on metal*, which generally do not require subsequent metallization. First, we revisit the works that employ a 3-D printing in plastic and then apply a conductivity layer all over their surface. This manufacturing option is the most common in the literature for the fabrication of 3-D metamaterials. Several examples of this type of 3-D manufacturing can be seen in the prototypes of the following [125,126,134–136,161,164,175–180]. Different technologies related to plastic 3-D printing are also available and some of them were used in previous work. Fused filament fabrication or *fused deposition modeling* (FDM) is the most common for general-purpose 3-D printers. It is based on the fusion of a thermoplastic in which the extruder nozzle produces the printed piece. Prototypes presented in [175,178] use 3-D printers based on FDM in which the thermoplastic filaments are *polylactic acid* (PLA) and *acrylonitrile butadiene styrene* (ABS). Figure 4a shows the prototype in the work by [178], where a cross-section of the unit cell

clearly shows how it was manufactured. Another 3-D printing technology presented in the above studies is the one based on *material jetting* (MJ), in which the principle of operation is based on the deposition of material droplets in each layer that are cured by UV light before another layer is printed. This type of 3-D printing technique is used in [134–136], and Figure 4b reveals the cross-section of the unit cell reported in [135]. Similar to the previous 3-D printing technology, it is the 3-D printing based on *stereolithography* (SLA). The similarity lies in the use of UV light to cure the material (in this case, resin) layer by layer. However, the difference between both of them is that the SLA makes the cure in a tank full of resin while MJ cures the material after the material has been sprayed. Unit cell designs that have employed SLA in their prototyping are presented in [126,161,164,176,179,180]. The last technology applied for the manufacture of 3-D metamaterials using 3-D printing on plastic is called *selective laser sintering* (SLS) used in [125,177]. In contrast with the previous 3-D printing technologies, this one sinters and fuses a preheat polymer powder by a laser to create the printed piece. The latter uses nylon as the sinterized material in the 3-D printing process. Since the 3-D printing technologies described above print the unit cells on plastic and they have conceived to be metallic, a metallization process is needed to coat the surface of the printed unit cells with a highly conductive metal. Different techniques to metallize the surface of the unit cells have been seen in previous work: brush paint [136,177], spray [164], electroplating [178,180], electroless plating [175], sputtering [134,176], dip coating [125], and vacuum chamber metallization [179]. Metallization is a crucial part of this manufacturing process as each of the above techniques offers a level of roughness, conductivity, and layer thickness that must be taken into account depending on the operating frequency range and geometry of the unit cell. It is important to mention that 3-D printing on plastic has been also extensively employed in fully dielectric unit cells in the lens design [173,174]. To end with 3-D printing techniques, there exists an alternative 3-D printing process that prints directly on metal and, thus, avoids the metallization process. Few studies in the literature have employed this 3-D printing technique. In [131], a 3-D metamaterial printed on a cobalt–chromium alloy by *selective laser melting* (SLM) was presented. In contrast to the previous work, in [94], the same 3-D printing technique was used but the printed metal was titanium. The choice of this type of metal instead of other metals such as aluminum alloys lies in the fact that it is possible to achieve a higher precision in the metal printing. Nevertheless, SLM needs high control and power in the laser since it has to reach the melting point of the printed metal, contrary to the similar 3-D printing technique named *direct metal laser sintering* (DMLS), where the metal powder is preheated and the laser power does not need to be as high as in SLM.

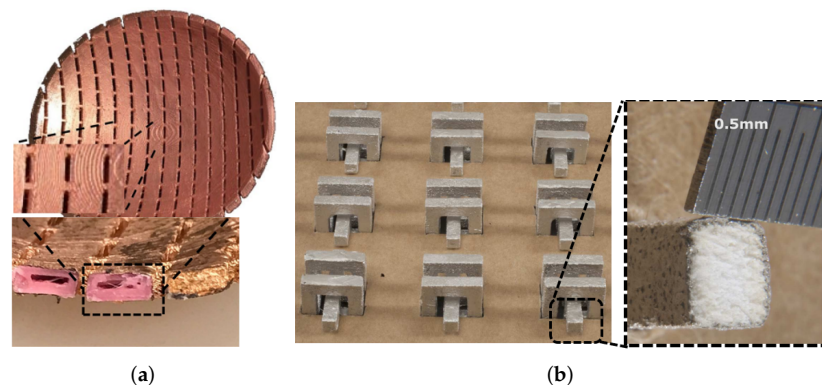


Figure 4. Examples of 3-D metamaterials manufactured by 3-D printing with subsequent metallization. (a) Design from [178] fabricated using FDM and electroplating. (b) Design from [135] fabricated using MJ and silver coating.

4.3. Alternative Techniques for 3-D Prototyping

Although 3-D assembly and 3-D printing techniques have proven to be very successful, other manufacturing alternatives can be also found in the literature to produce 3-D metamaterials. In [181], *water transfer printing* (WPT) technology was employed to successfully transfer a metasurface into a 3-D metal mold. Before using the WPT, the metasurface was manufactured by *inkjet printing* on a flexible substrate such as polyethylene terephthalate (PET). With the use of WPT, the unit cells achieve a 3-D shape due to the mold geometry. The design presented in [182] produced a 3-D FSS constituted by folded dipoles that are inkjet printed on a cellulose paper. This was selected as a flexible substrate of the prototype because it can produce origami patterns that are inherently 3-D structures. Instead of using flexible substrates, as in the previous work, in [183], FDM was used to create a 3-D structure, and then, cross dipoles and square loops were printed with metallic ink. For 3-D metamaterial that were intended to operate at terahertz frequencies, nanometer-precision manufacturing techniques were needed for functional prototyping. The work in [184–186] used fabrication techniques based on *lithography* to achieve these levels of manufacturing precision. As a summary, Table 2 presents all of the papers presented in this section.

Table 2. Summary of the fabrication characteristics of the studies mentioned in Section 4.

Works	Fabrication Technique	3-D Assembly	Required Metallization
[138,141–143,146,147,156,163]	PCB fabrication	Yes	No *
[9]	EDM	No	No
[175,178]	FDM 3-D printing	No	Yes
[134–136]	MJ 3-D printing	No	Yes
[126,161,164,176,179,180]	SLA 3-D printing	No	Yes
[125,177]	SLS 3-D printing	No	Yes
[94,131]	SLM 3-D printing	No	No
[181]	Inkjet printing and WPT	No	No
[182]	Inkjet printing on origami structures	No	No
[183]	Inkjet printing and FDM	No	No
[184–186]	Lithography	No	Yes

* It may require soldering or conductive bonding to ensure electrical continuity.

5. Future Trends

Thus far, we presented an overview of the existing computational methods, designs, and manufacturing techniques related to 3-D metamaterials, particularly in for microwave and photonic regimes. Nonetheless, times are evolving and some of the formerly discussed ideas may become obsolete in the future while others may have incredible potential, such as the application of artificial intelligence algorithms. Here, we present our vision on future trends and challenges in the field of 3-D metamaterials.

Computational complexity increases notably when considering 3-D metamaterials compared with traditional 1-D and 2-D metasurfaces. Furthermore, 3-D geometries are substantially more difficult to model than planar configurations. As a direct consequence, gaining physical insight into the electromagnetic behavior of the structure is becoming increasingly complex. Certainly, FEM and finite difference methods are very appreciated generalist approaches, as they can deal with all types of geometries and materials, normally at the expense of higher

computational resources and a lack of physical insight. Thus, those methods (or hybrids) that reduce computation times and, at the same time, provide physical insight will attract much attention for the analysis of 3-D structures. This is the case of reduced-order models such as equivalent circuits, ray optics, and homogenization methods. Ray optics and homogenization techniques are not new to 3-D metamaterials, even though their capabilities have not been fully exploited. However, circuit models applied to 3-D structures are rarely found in the literature. It is a field to be developed due to its enormous potential. On the other hand, modal techniques are intermediate solutions between purely numerical approaches and reduced-order models. They offer a good performance in most of the features highlighted in Table 1. Actually, Floquet modal expansions (together with FDTD and homogenization methods) are the first techniques to be implemented for the analysis of *spacetime metamaterials* (periodic configurations modulated in space and time) [187–189], which is one of the current hot topics in electromagnetism [190–192]. In fact, current commercial software fail to consider time modulations in the computation, so in-house codes are needed to model spacetime structures. Additionally, *artificial intelligence* (AI) has supposed a breakthrough in electromagnetics and electronics in solving challenging problems (scattering, radar, channel parameter estimation, microwave imaging, remote sensing, etc.) involving a large number of variables and design constraints [193–197]. In the near future, it is expected that AI techniques such as machine learning or deep neural networks coexist with the more traditional computational methods reviewed in this document.

In the context of cell designs and potential functionalities in the short and intermediate term, a clear trend is determined by 5G and 6G communication standards. Specially the leverage of millimeter bands, where terminals must adequately be adapted to the operation wavelength. The use of dielectric materials becomes problematic at these frequencies due to the strong presence of losses. The use of 3-D fully metallic devices is expected to be widespread, as long as the contemporaneous fabrication techniques correspondingly evolved. This need for full-metal structures is shared by spatial-applications demands [198], since spacial environments are exposed to very extreme conditions (thermal, electromagnetics, etc.). At the same time, 3-D metamaterials allows for a *perfect* decoupling between vertical and horizontal polarizations. This motivates the search for and improvement in functionalities and applications where the control of both field components must be carefully controlled. Such is the case of circular polarizers, polarization converters, absorbers, etc. The design of dual-pol absorbers, in particular those called rasorbers for radar scenarios, deserve special attention. The independent control of both polarizations would induce reflection/absorption independent channels for each of them. Three-dimensional structures are also incorporated into the field of *reconfigurable intelligent surfaces* (RIS), where the strict control of field patterns emitted by the metasurface is realized via reconfiguration. Despite the bulk of research relying on a reconfigurable material (especially to operate at millimeter bands without loss of efficiency), the effective number of field patterns increases when both polarizations are relevant instead of one. Three-dimensional metasurfaces are therefore good candidates for future RIS [8] and the promising contexts where RIS will be applied, e.g., the intelligent vehicle [199] and vortex-generation for RF imaging systems [200], etc.

Regarding the manufacturing techniques employed for the production of 3-D metamaterials, Table 2 clearly shows that the two that are mainly used are PCB fabrication with a 3-D assembly and 3-D printing in plastic (FDM, MJ, SLA, and SLS) with subsequent metallization. PCB fabrication has been one of the most developed manufacturing techniques in recent decades due to its wide use in integrated circuits. Nevertheless, the designs prototyped with PCB technique always require a 3-D assembly and the presence of a substrate, which significantly increase the dielectric losses at millimeter-wave frequencies. On the other hand, due to the great recent development of 3-D printing in recent years, a great diversity of high-precision

and cost-effective 3-D printers can be found. As a consequence, 3-D printing is intensively applied nowadays for the production of high-frequency RF prototypes. However, it has the disadvantage of requiring metallization, which becomes complex for small details and low roughness. This is evidenced by the diversity of metal plating techniques used in the studies mentioned in Section 4 related to 3-D printing on plastics. Therefore, it is necessary to further improve the abovementioned manufacturing techniques. One of the envisaged solutions is the possibility of low-cost 3-D printing in metals, producing a low level of roughness and a good conductivity desired for 3-D metamaterials at millimeter-wave regime. These characteristics in the manufacturing would eliminate the need for metallization, even though a subsequent metallization is sometimes required to either increase the conductivity of the base metal or to minimize the surface roughness of the printed prototype [201].

6. Conclusions

In this paper, we presented an overview of the past, present, and future challenges related to 3-D metamaterials. We introduced the main limitations that have prevented 3-D metamaterials to be properly utilized in the past, as well as the advantages that 3-D configurations can offer compared with their 1-D and 2-D counterparts.

First, we reviewed the most relevant computational methods applied to 3-D metamaterial design. Table 1 summarizes the main features of these methods. In terms of generality of use, robustness, and accuracy, finite difference, finite element, and integral-equation methods are the most applicable, normally at the cost of higher computational resources and lack of physical insight. Modal techniques and reduced-order models (circuits, ray tracing, and homogenization) provide faster computation times and physical insight on electromagnetic phenomena, typically in exchange for lower flexibility and accuracy in the computation. These computational methods have been efficiently applied in a wide variety of periodic and truncated 3-D configurations, such as nanoparticle systems, EBG structures, wire media, cavities, chiral elements, and cloaking devices.

Second, we presented an overview of the most outstanding designs and inherent functionalities of 3-D metamaterials. A wide range of applications can be covered, from classical filters to novel metasurfaces for polarization control. Three-dimensional architectures have been theorized for several decades, but the *massive* experimental exploitation comes from the beginning of the current century. In this sense, they originally played an important role in the discovery and development of metamaterials thanks to the exotic electrical properties of 3-D distributions of split-ring resonators. The existing advantages with respect to classical 2-D designs makes 3-D structures potential candidates for operation in future applications, especially in spacial environments and beyond millimeter frequencies, where dielectric materials are undesired. The work realized and published during the last decade has demonstrated that low-profile 3-D metamaterials/metasurfaces may already cover a wide variety of functionalities. The development of novel 3-D devices and prototypes is therefore expected to increase and to be refined due to the permanent improvement in 3D-printing techniques, leading to a new scenario in the fields of telecommunications.

Finally, we discussed on the current fabrication techniques for the prototyping of 3-D metamaterials. A wide variety of manufacturing techniques have been used in the work reported in the literature. Of all those found, the most relevant are PCB fabrication, which requires a mandatory three-dimensional assembly of the fabricated layers, and 3-D printing, which by its nature fits the 3-D geometries that appear in the unit cells of the metamaterials. Regarding the latter, 3-D printing in plastic with a subsequent metallization is the manufacturing strategy that predominates in the reviewed works, essentially due to the reduced cost compared with direct 3-D printing on metal.

Author Contributions: Conceptualization, A.A.-A. and C.M.; computational methods (Section 2), A.A.-A.; designs (Section 3), C.M.; fabrication techniques (Section 4), Á.P.-C.; introduction and future trends (Sections 1 and 5), A.A.-A., Á.P.-C., and C.M. All authors reviewed and edited the document. All authors have read and agreed to the published version of the manuscript.

Funding: This work was funded in part by the Predoctoral Grant FPU18/01965 and in part by the financial support of BBVA Foundation through a project belonging to the 2021 Leonardo Grants for Researchers and Cultural Creators, BBVA Foundation. The BBVA Foundation accepts no responsibility for the opinions, statements, and contents included in the project and/or the results thereof, which are entirely the responsibility of the authors.

Institutional Review Board Statement: Not applicable

Informed Consent Statement: Not applicable

Data Availability Statement: Not applicable

Conflicts of Interest: The authors declare no conflicts of interest.

References

1. Smith, D.R.; Pendry, J.B.; Wiltshire, M.C.K. Metamaterials and Negative Refractive Index. *Science* **2004**, *305*, 788–792.
2. Engheta, N.; Ziolkowski, R.W. *Metamaterials: Physics and Engineering Explorations*; Wiley-IEEE Press: Hoboken, New Jersey, USA, 2006.
3. Liu, Y.; Zhang, X. Metamaterials: A new frontier of science and technology. *Chem. Soc. Rev.* **2011**, *40*, 2494–2507.
4. Chen, H.T.; Taylor, A.J.; Yu, N. A review of metasurfaces: Physics and applications. *Rep. Prog. Phys.* **2016**, *79*, 076401. <https://doi.org/10.1088/0034-4885/79/7/076401>.
5. Quevedo-Teruel, O.; et al. Roadmap on metasurfaces. *J. Opt.* **2019**, *21*, 073002. <https://doi.org/10.1088/2040-8986/ab161d>.
6. Kadic, M.; Milton, G.; van Hecke, M.; Wegener, M. 3D Metamaterials. *Nat. Rev. Phys.* **2019**, *1*, 198–210.
7. Gabriele G.; Di Renzo, M.; Diaz-Rubio, A.; Tretyakov, S.; Caloz, C.; Peng, Z.; Alu, A.; Lerosey, G.; Fink, M.; Galdi, V.; et al. Smart Radio Environments. *arXiv* **2021**, arXiv:2111.08676.
8. Molero, C.; Palomares-Caballero, Á.; Alex-Amor, A.; Parellada-Serrano, I.; Gamiz, F.; Padilla, P.; Valenzuela-Valdés, J.F. Metamaterial-Based Reconfigurable Intelligent Surface: 3D Meta-Atoms Controlled by Graphene Structures. *IEEE Commun. Mag.* **2021**, *59*, 42–48. <https://doi.org/10.1109/MCOM.001.2001161>.
9. Molero Jimenez, C.; Menargues, E.; García-Vigueras, M. All-Metal 3-D Frequency-Selective Surface With Versatile Dual-Band Polarization Conversion. *IEEE Trans. Antennas Propag.* **2020**, *68*, 5431–5441. <https://doi.org/10.1109/TAP.2020.2975270>.
10. Al Sabouni-Zawadzka, A.; Gilewski, W. Soft and Stiff Simplex Tensegrity Lattices as Extreme Smart Metamaterials. *Materials* **2019**, *12*, 187. <https://doi.org/10.3390/ma12010187>.
11. Reinbold, J.; Frenzel, T.; Münchinger, A.; Wegener, M. The Rise of (Chiral) 3D Mechanical Metamaterials. *Materials* **2019**, *12*, 3527.
12. Wu, W.; Hu, W.; Qian, G.; Liao, H.; Xu, X.; Berto, F. Mechanical design and multifunctional applications of chiral mechanical metamaterials: A review. *Mater. Des.* **2019**, *180*, 107950.
13. Gorshkov, V.; Sareh, P.; Navadeh, N.; Tereshchuk, V.; Fallah, A.S. Multi-resonator metamaterials as multi-band metastructures. *Mater. Des.* **2021**, *202*, 109522.
14. Georgakopoulos, S.V.; Zekios, C.L.; Sattar-Kaddour, A.; Hamza, M.; Biswas, A.; Clark, B.; Ynchausti, C.; Howell, L.L.; Magleby, S.P.; Lang, R.J. Origami Antennas. *IEEE Open J. Antennas Propag.* **2021**, *2*, 1020–1043.
15. Wang, H.; Chen, Q.; Zetterstrom, O.; Quevedo-Teruel, O. Three-Dimensional Broadband and Isotropic Double-Mesh Twin-Wire Media for Meta-Lenses. *Appl. Sci.* **2021**, *11*, 7153.
16. Chen, Z.; Wang, C.-F.; Hoefer, W.J.R. A Unified View of Computational Electromagnetics. *IEEE Trans. Microw. Theory Tech.* **2022**. <https://doi.org/10.1109/TMTT.2021.3138911>.
17. Jones, D.S. *Methods in Electromagnetic Wave Propagation*; Clarendon Press; Oxford University Press: New York, NY, USA, 1979.
18. Tan, E.L. Unconditionally Stable LOD-FDTD Method for 3-D Maxwell's Equations. *IEEE Microw. Wirel. Compon. Lett.* **2007**, *17*, 85–87. <https://doi.org/10.1109/LMWC.2006.890166>.
19. Elsherbeni, A.Z.; Demir, V. *The Finite-Difference Time-Domain Method for Electromagnetics with MATLAB*; SciTech Publishing, Inc.: Raleigh, NC, USA, 2015.
20. Yee, K. Numerical solution of initial boundary value problems involving maxwell's equations in isotropic media. *IEEE Trans. Antennas Propag.* **1966**, *14*, 302–307. <https://doi.org/10.1109/TAP.1966.1138693>.
21. Shin, W. 3D Finite-Difference Frequency-Domain Method for Plasmonics and Nanophotonics. Ph.D. Thesis, Stanford University, Stanford, CA, USA, 2013.

22. Aoki, K.; Guimard, D.; Nishioka, M.; Nomura, M.; Iwamoto, S.; Arakawa, Y. Coupling of quantum-dot light emission with a three-dimensional photonic-crystal nanocavity. *Nat. Photonics* **2008**, *2*, 688–692. <https://doi.org/10.1038/nphoton.2008.202>.
23. Ho, Y.L.D.; Ivanov, P.S.; Engin, E.; Nicol, M.F.J.; Taverne, M.P.C.; Hu, C.; Cryan, M.J.; Craddock, I.J.; Railton, C.J.; Rarity, J.G. FDTD Simulation of Inverse 3-D Face-Centered Cubic Photonic Crystal Cavities. *IEEE J. Quantum Electron.* **2011**, *47*, 1480–1492. <https://doi.org/10.1109/JQE.2011.2170404>.
24. Zheng, X.; Taverne, M.P.C.; Ho, Y.L.D.; Rarity, J.G. Cavity Design in Woodpile Based 3D Photonic Crystals. *Appl. Sci.* **2018**, *8*, 1087. <https://doi.org/10.3390/app8071087>.
25. Rumpf, R. Simple implementation of arbitrarily shaped total-field/scattered-field regions in finite-difference frequency-domain. *Prog. Electromagn. Res. B* **2011**, *36*, 221–248. <https://doi.org/10.2528/PIERB11092006>.
26. Rumpf, R.; Garcia, C.; Berry, E.; Barton, J. Finite-Difference Frequency-Domain Algorithm for Modeling Electromagnetic Scattering From General Anisotropic Objects. *Prog. Electromagn. Res. B* **2014**, *61*, 55–67. <https://doi.org/10.2528/PIERB14071606>.
27. Ivinskaya, A.M.; Lavrinenko, A.V.; Shyroki, D.M. Modeling of Nanophotonic Resonators With the Finite-Difference Frequency-Domain Method. *IEEE Trans. Antennas Propag.* **2011**, *59*, 4155–4161.
28. Silvester, P.P.; Ferrari, R.L. *Finite Elements for Electrical Engineers*, 3rd ed.; Cambridge University Press: Cambridge, UK, 1996. <https://doi.org/10.1017/CBO9781139170611>.
29. Zhai, Y.B.; Ping, X.W.; Jiang, W.X.; Cui, T.J. Finite-Element Analysis of Three-Dimensional Axisymmetrical Invisibility Cloaks and Other Metamaterial Devices. *Commun. Comput. Phys.* **2010**, *8*, 823–834.
30. Burger, S.; Klose, R.; Schaedle, A.; Schmidt, F.; Zschiedrich, L. FEM modeling of 3D photonic crystals and photonic crystal waveguides. *Proc. SPIE—Int. Soc. Opt. Eng.* **2005**, 1–10. <https://doi.org/10.1117/12.585895>.
31. Frenzel, T.; Hahn, V.; Ziemke, P.; Schneider, J.; Chen, Y.; Kiefer, P.; Gumbsch, P.; Wegener, M. Large characteristic lengths in 3D chiral elastic metamaterials. *Commun. Mater.* **2021**, *2*, 4. <https://doi.org/10.1038/s43246-020-00107-w>.
32. COMSOL AB. COMSOL Multiphysics. Available online: <https://www.comsol.com/comsol-multiphysics> (accessed on 27 January 2022).
33. Adrian, S.B.; Dély, A.; Consoli, D.; Merlini, A.; Andriulli, F.P. Electromagnetic Integral Equations: Insights in Conditioning and Preconditioning. *IEEE Open J. Antennas Propag.* **2021**, *2*, 1143–1174.
34. Burton, A.J.; Miller, G.F.; Wilkinson, J.H. The application of integral equation methods to the numerical solution of some exterior boundary-value problems. *Proc. R. Soc. Lond. A. Math. Phys. Sci.* **1971**, *323*, 201–210.
35. Volakis, J.L.; Sertel, K. *Integral Equation Methods for Electromagnetics*; Scitech Publishing Inc.: Raleigh, NJ, USA, 2012.
36. Gibson, W.C. *The Method of Moments in Electromagnetics*, 3rd ed.; Chapman and Hall/CRC: Boca Raton, FL, USA, 2021.
37. Paez-Rueda, C.-I. Fajardo, A. Pérez, M.; Perilla, G. Closed-Form Expressions for Numerical Evaluation of Self-Impedance Terms Involved on Wire Antenna Analysis by the Method of Moments. *Electronics* **2021**, *10*, 1316.
38. González-Ovejero, D.; Maci, S. Gaussian Ring Basis Functions for the Analysis of Modulated Metasurface Antennas. *IEEE Trans. Antennas Propag.* **2015**, *63*, 3982–3993.
39. Florencio, R.; Boix, R.R.; Encinar, J.A. Efficient Spectral Domain MoM for the Design of Circularly Polarized Reflectarray Antennas Made of Split Rings. *IEEE Trans. Antennas Propag.* **2019**, *67*, 1760–1771.
40. Florencio, R.; Boix, R.R.; Encinar, J.A. Enhanced MoM Analysis of the Scattering by Periodic Strip Gratings in Multilayered Substrates. *IEEE Trans. Antennas Propag.* **2013**, *61*, 5088–5099. <https://doi.org/10.1109/TAP.2013.2273213>.
41. Florencio, R.; Somolinos, Á; González, I.; Cátedra, F.; Lozano, L. Comparison between Specialized Quadrature Rules for Method of Moments with NURBS Modelling Applied to Periodic Multilayer Structures. *Electronics* **2020**, *9*, 2043. <https://doi.org/10.3390/electronics9122043>.
42. Florencio, R.; Somolinos, Á; González, I.; Cátedra, F. Fast Preconditioner Computation for BICGSTAB-FFT Method of Moments with NURBS in Large Multilayer Structures. *Electronics* **2020**, *9*, 1938. <https://doi.org/10.3390/electronics9111938>.
43. Córcoles, J.; Boix, R.R. Spectral MoM NUFFT-Based Formulation for the Efficient Analysis of High-Order Bandpass FSSs With Tightly Packed Nonresonant Elements in Skewed Grid. *IEEE Trans. Antennas Propag.* **2021**, *69*, 6099–6104.
44. Silveirinha, M.; Fernandes, C. A hybrid method for the efficient calculation of the band structure of 3-D metallic crystals. *IEEE Trans. Microw. Theory Tech.* **2004**, *52*, 889–902. <https://doi.org/10.1109/TMTT.2004.823563>.
45. Tihon, D.; Sozio, V.; Ozdemir, N.A.; Albani, M.; Craeye, C. Numerically Stable Eigenmode Extraction in 3-D Periodic Metamaterials. *IEEE Trans. Antennas Propag.* **2016**, *64*, 3068–3079. <https://doi.org/10.1109/TAP.2016.2562659>.
46. Tong, M.S.; Chew, W.C. *The Nystrom Method in Electromagnetics*; Wiley-IEEE Press: Hoboken, New Jersey, USA, 2020.
47. Tong, M.S.; Qian, Z.G.; Chew, W.C. Nyström Method Solution of Volume Integral Equations for Electromagnetic Scattering by 3D Penetrable Objects. *IEEE Trans. Antennas Propag.* **2010**, *58*, 1645–1652.
48. Chen, D.; Cho, M.H.; Cai, W. Accurate and Efficient Nyström Volume Integral Equation Method for Electromagnetic Scattering of 3-D Metamaterials in Layered Media. *SIAM J. Sci. Comput.* **2018**, *40*, B259–B282.
49. Engheta, N.; Murphy, W.D.; Rokhlin, V.; Vassiliou, M.S. The Fast Multipole Method (FMM) for Electromagnetic Scattering Problems. *IEEE Trans. Antennas Propag.* **1992**, *40*, 634–641.

50. Darve, E. The Fast Multipole Method: Numerical Implementation. *J. Comput. Phys.* **2000**, *160*, 195–240.
51. Fall, M.; Boutami, S.; Glière, A.; Stout, B.; Hazart, J. Multilevel fast multipole method based on a potential formulation for 3D electromagnetic scattering problems. *J. Opt. Soc. Am. A* **2013**, *30*, 1273–1280.
52. Daniele, V.; Zich, R. *The Wiener-Hopf Method in Electromagnetics*; Scitech Publishing: Edison, NJ, USA, 2014.
53. Albani, M.; Capolino, F. Wave dynamics by a plane wave on a half-space metamaterial made of plasmonic nanospheres: A discrete Wiener–Hopf formulation. *J. Opt. Soc. Am. B* **2011**, *28*, 2174–2185.
54. Camacho, M.; Hibbins, A.P.; Capolino, F.; Albani, M. Diffraction by a truncated planar array of dipoles: A Wiener–Hopf approach. *Wave Motion* **2019**, *89*, 28–42.
55. Arens, T.; Sandfort, K.; Schmitt, S.; Lechleiter, A. Analysing Ewald’s method for the evaluation of Green’s functions for periodic media. *IMA J. Appl. Math.* **2011**, *78*, 405–431.
56. Campione, S.; Capolino, F. Ewald method for 3D periodic dyadic Green’s functions and complex modes in composite materials made of spherical particles under the dual dipole approximation. *Radio Sci.* **2012**, *47*, RS0N06.
57. Campione, S.; Capolino, F. Electromagnetic coupling and array packing induce exchange of dominance on complex modes in 3D periodic arrays of spheres with large permittivity. *J. Opt. Soc. Am. B* **2016**, *33*, 261–270.
58. Stevanoviæ, I.; Mosig, J.R. Periodic Green’s function for skewed 3-D lattices using the Ewald transformation. *Microw. Opt. Technol. Lett.* **2007**, *49*, 1353–1357.
59. Wexler, A. Solution of Waveguide Discontinuities by Modal Analysis. *IEEE Trans. Microw. Theory Tech.* **1967**, *15*, 508–517.
60. Collin, R.E. *Field Theory of Guided Waves*, 2nd ed.; IEEE-Press: New York, NY, USA, 1991.
61. Ruiz-Cruz, J.A.; Montejo-Garai, J.R.; Rebollar, J.M. Computer Aided Design of Waveguide Devices by Mode-Matching Methods. In *Passive Microwave Components and Antennas*; Zhurbenko, V., Ed.; IntechOpen: Rijeka, Croatia, 2010; Chapter 6.
62. Swartz, K.E.; White, D.A.; Tortorelli, D.A.; James, K.A. Topology optimization of 3D photonic crystals with complete bandgaps. *Opt. Express* **2021**, *29*, 22170–22191. <https://doi.org/10.1364/OE.427702>.
63. Ghadarghadr, S.; Mosallaei, H. Dispersion Diagram Characteristics of Periodic Array of Dielectric and Magnetic Materials Based Spheres. *IEEE Trans. Antennas Propag.* **2009**, *57*, 149–160. <https://doi.org/10.1109/TAP.2008.2009725>.
64. Campione, S.; Steshenko, S.; Albani, M.; Capolino, F. Complex modes and effective refractive index in 3D periodic arrays of plasmonic nanospheres. *Opt. Express* **2011**, *19*, 26027–26043. <https://doi.org/10.1364/OE.19.026027>.
65. Varela, J.E.; Esteban, J. Characterization of Waveguides With a Combination of Conductor and Periodic Boundary Contours: Application to the Analysis of Bi-Periodic Structures. *IEEE Trans. Microw. Theory Tech.* **2012**, *60*, 419–430.
66. Dai, Q.I.; Lo, Y.H.; Chew, W.C.; Liu, Y.G.; Jiang, L.J. Generalized Modal Expansion and Reduced Modal Representation of 3-D Electromagnetic Fields. *IEEE Trans. Antennas Propag.* **2014**, *62*, 783–793.
67. Rabinovich, O.; Epstein, A. Dual-Polarized All-Metallic Metagratings For Perfect Anomalous Reflection. *Phys. Rev. Appl.* **2020**, *14*, 064028. <https://doi.org/10.1103/PhysRevApplied.14.064028>.
68. Kari, N.; Seetharamdoo, D.; Laheurte, J.M.; Sarrazin, F. Modal Analysis of Chiral Metamaterial Using Characteristic Mode Analysis and Eigenmode Expansion Method. *IEEE J. Multiscale Multiphys. Comput. Tech.* **2020**, *5*, 37–43. <https://doi.org/10.1109/JMMCT.2020.2981235>.
69. Alex-Amor, A.; Ghasemifard, F.; Valerio, G.; Ebrahimpouri, M.; Padilla, P.; González, J.M.F.; Quevedo-Teruel, O. Glide-Symmetric Metallic Structures With Elliptical Holes for Lens Compression. *IEEE Trans. Microw. Theory Tech.* **2020**, *68*, 4236–4248.
70. Alex-Amor, A.; Valerio, G.; Ghasemifard, F.; Mesa, F.; Padilla, P.; Fernández-González, J.M.; Quevedo-Teruel, O. Wave Propagation in Periodic Metallic Structures with Equilateral Triangular Holes. *Appl. Sci.* **2020**, *10*, 1600. <https://doi.org/10.3390/app10051600>.
71. Zetterstrom, O.; Valerio, G.; Mesa, F.; Ghasemifard, F.; Norgren, M.; Quevedo-Teruel, O. Dispersion Analysis of Periodically Loaded Transmission Lines with Twist Symmetry Using the Mode-Matching Technique. *Appl. Sci.* **2020**, *10*, 5990. <https://doi.org/10.3390/app10175990>.
72. Sipus, Z.; Bosiljevac, M. Modeling of Glide-Symmetric Dielectric Structures. *Symmetry* **2019**, *11*, 805. <https://doi.org/10.3390/sym11060805>.
73. Marcuvitz, N. *Waveguide Handbook*; Electromagnetic Waves, Institution of Engineering and Technology: New York, McGraw-Hill, 1986.
74. Mesa, F.; Rodriguez-Berral, R.; Medina, F. Unlocking Complexity Using the ECA: The Equivalent Circuit Model as An Efficient and Physically Insightful Tool for Microwave Engineering. *IEEE Microw. Mag.* **2018**, *19*, 44–65. <https://doi.org/10.1109/MMM.2018.2813821>.
75. Costa, F.; Monorchio, A.; Manara, G. An Overview of Equivalent Circuit Modeling Techniques of Frequency Selective Surfaces and Metasurfaces. *Appl. Comput. Electromagn. Soc. J.* **2014**, *29*, 960–976.
76. Kafesaki, M.; Tsiapa, I.; Katsarakis, N.; Koschny, T.; Soukoulis, C.M.; Economou, E.N. Left-handed metamaterials: The fishnet structure and its variations. *Phys. Rev. B* **2007**, *75*, 235114.
77. Carbonell, J.; Croëne, C.; Garet, F.; Lheurette, E.; Coutaz, J.L.; Lippens, D. Lumped elements circuit of terahertz fishnet-like arrays with composite dispersion. *J. Appl. Phys.* **2010**, *108*, 014907.
78. Perez-Palomino, G.; Page, J.E. Bimode Foster’s Equivalent Circuit of Arbitrary Planar Periodic Structures and Its Application to Design Polarization Controller Devices. *IEEE Trans. Antennas Propag.* **2020**, *68*, 5308–5321.

79. Borgese, M.; Costa, F. A Simple Equivalent Circuit Approach for Anisotropic Frequency-Selective Surfaces and Metasurfaces. *IEEE Trans. Antennas Propag.* **2020**, *68*, 7088–7098.
80. Hernández-Escobar, A.; Abdo-Sánchez, E.; Esteban, J.; Martín-Guerrero, T.M.; Camacho-Peñalosa, C. Equivalent-Circuit Modeling of Lossless and Lossy Bi-Periodic Scatterers by an Eigenstate Approach. 2021. <https://doi.org/10.36227/techrxiv.16811092.v1>.
81. Rodríguez-Berral, R.; Mesa, F.; Medina, F. Analytical Multimodal Network Approach for 2-D Arrays of Planar Patches/Apertures Embedded in a Layered Medium. *IEEE Trans. Antennas Propag.* **2015**, *63*, 1969–1984.
82. Astorino, M.D.; Frezza, F.; Tedeschi, N. Equivalent-circuit model for stacked slot-based 2D periodic arrays of arbitrary geometry for broadband analysis. *J. Appl. Phys.* **2018**, *123*, 103106.
83. Hum, S.V.; Du, B. Equivalent Circuit Modeling for Reflectarrays Using Floquet Modal Expansion. *IEEE Trans. Antennas Propag.* **2017**, *65*, 1131–1140.
84. Omar, S.; Jiao, D. A New Volume Integral Formulation for Broadband 3-D Circuit Extraction in Inhomogeneous Materials With and Without External Electromagnetic Fields. *IEEE Trans. Microw. Theory Tech.* **2013**, *61*, 4302–4312.
85. Omar, S.; Jiao, D. A Linear Complexity Direct Volume Integral Equation Solver for Full-Wave 3-D Circuit Extraction in Inhomogeneous Materials. *IEEE Trans. Microw. Theory Tech.* **2015**, *63*, 897–912.
86. Molero, C.; Alex-Amor, A.; Mesa, F.; Palomares-Caballero, A.; Padilla, P. Cross-Polarization Control in FSSs by Means of an Equivalent Circuit Approach. *IEEE Access* **2021**, *9*, 99513–99525. <https://doi.org/10.1109/ACCESS.2021.3096715>.
87. Alex-Amor, A.; Mesa, F.; Palomares-Caballero, Á.; Molero, C.; Padilla, P. Exploring the Potential of the Multi-Modal Equivalent Circuit Approach for Stacks of 2-D Aperture Arrays. *IEEE Trans. Antennas Propag.* **2021**, *69*, 6453–6467. <https://doi.org/10.1109/TAP.2021.3070150>.
88. Grbic, A.; Eleftheriades, G.V. An isotropic three-dimensional negative-refractive-index transmission-line metamaterial. *J. Appl. Phys.* **2005**, *98*, 043106. <https://doi.org/10.1063/1.2007853>.
89. Zedler, M.; Caloz, C.; Russer, P. A 3-D Isotropic Left-Handed Metamaterial Based on the Rotated Transmission-Line Matrix (TLM) Scheme. *IEEE Trans. Microw. Theory Tech.* **2007**, *55*, 2930–2941. <https://doi.org/10.1109/TMTT.2007.909608>.
90. Zedler, M.; Russer, P. Investigation on the Dispersion Relation of a 3D LC-based Metamaterial with an Omnidirectional Left-Handed Frequency Band. In Proceedings of the 2006 IEEE MTT-S International Microwave Symposium Digest, San Francisco, CA, USA, 11–16 June 2006; pp. 1477–1479.
91. Johns, P.B. A Symmetrical Condensed Node for the TLM Method. *IEEE Trans. Microw. Theory Tech.* **1987**, *35*, 370–377.
92. Molero, C.; García-Vigueras, M. Circuit Modeling of 3-D Cells to Design Versatile Full-Metal Polarizers. *IEEE Trans. Microw. Theory Tech.* **2019**, *67*, 1357–1369. <https://doi.org/10.1109/TMTT.2019.2898828>.
93. Balmaseda-Marquez, M.; Moreno, S.; Zapata, P.H.; Molero, C. Phase-resonance Exploitation in Full-Metal 3D Periodic Structures for Single- and Multi- Wideband Applications. *Techrxiv* **2021**. <https://doi.org/10.36227/techrxiv.17439956.v1>.
94. Molero, C.; Legay, H.; Pierre, T.; Garcia-Vigueras, M. Broadband 3D-Printed Polarizer based on Metallic Transverse Electro-Magnetic Unit-Cells. *IEEE Trans. Antennas Propag.* **2022**. <https://doi.org/10.1109/TAP.2022.3145435>.
95. Blanchard, J.; Newman, E.; Peters, M. Integral equation analysis of artificial media. *IEEE Trans. Antennas Propag.* **1994**, *42*, 727–731. <https://doi.org/10.1109/8.299573>.
96. Silveirinha, M.; Fernandes, C. Homogenization of 3-D-connected and nonconnected wire metamaterials. *IEEE Trans. Microw. Theory Tech.* **2005**, *53*, 1418–1430. <https://doi.org/10.1109/TMTT.2005.845128>.
97. Silveirinha, M. Additional boundary condition for the wire medium. *IEEE Trans. Antennas Propag.* **2006**, *54*, 1766–1780.
98. Lannebère, S.; Morgado, T.A.; Silveirinha, M.G. First principles homogenization of periodic metamaterials and application to wire media. *Comptes Rendus. Physique* **2020**, *21*, 367–388.
99. Silveirinha, M.; Engheta, N. Design of matched zero-index metamaterials using nonmagnetic inclusions in epsilon-near-zero media. *Phys. Rev. B* **2007**, *75*, 075119. <https://doi.org/10.1103/PhysRevB.75.075119>.
100. Karamanos, T.D.; Assimonis, S.D.; Dimitriadis, A.I.; Kantartzis, N.V. Effective parameter extraction of 3D metamaterial arrays via first-principles homogenization theory. *Photonics-Nanostruct.—Fundam. Appl.* **2014**, *12*, 291–297.
101. Silveirinha, M.G. Metamaterial homogenization approach with application to the characterization of microstructured composites with negative parameters. *Phys. Rev. B* **2007**, *75*, 115104. <https://doi.org/10.1103/PhysRevB.75.115104>.
102. Fischer, B.; Valerio, G. Ultra-Wideband Homogenization of Glide-Symmetric Holey Parallel-Plate Waveguides. *IEEE Trans. Antennas Propag.* **2021**, *in press*.
103. Deschamps, G. Ray techniques in electromagnetics. *Proc. IEEE* **1972**, *60*, 1022–1035.
104. Xu, S.; Yang, F. Reflectarray Antennas. In *Handbook of Antenna Technologies*; Springer: Singapore, 2015.
105. Liao, Q.; Fonseca, N.J.G.; Quevedo-Teruel, O. Compact Multibeam Fully Metallic Geodesic Luneburg Lens Antenna Based on Non-Euclidean Transformation Optics. *IEEE Trans. Antennas Propag.* **2018**, *66*, 7383–7388. <https://doi.org/10.1109/TAP.2018.2872766>.
106. Fonseca, N.J.G.; Liao, Q.; Quevedo-Teruel, O. Equivalent Planar Lens Ray-Tracing Model to Design Modulated Geodesic Lenses Using Non-Euclidean Transformation Optics. *IEEE Trans. Antennas Propag.* **2020**, *68*, 3410–3422. <https://doi.org/10.1109/TAP.2020.2963948>.

107. Hossain, F.; Geok, T.K.; Rahman, T.A.; Hindia, M.N.; Dimyati, K.; Ahmed, S.; Tso, C.P.; Abd Rahman, N.Z. An Efficient 3-D Ray Tracing Method: Prediction of Indoor Radio Propagation at 28 GHz in 5G Network. *Electronics* **2019**, *8*, 286.
108. Solomitckii, D. *Evaluation of mmWave 5G Performance by Advanced Ray Tracing Techniques*; Academic Dissertation Tampere University, Faculty of Information Technology and Communication Sciences Finland, 2019.
109. Mesa, F.; Valerio, G.; Rodríguez-Berral, R.; Quevedo-Teruel, O. Simulation-Assisted Efficient Computation of the Dispersion Diagram of Periodic Structures: A comprehensive overview with applications to filters, leaky-wave antennas and metasurfaces. *IEEE Antennas Propag. Mag.* **2021**, *63*, 33–45.
110. Alex-Amor, A.; Palomares-Caballero, A.; Mesa, F.; Quevedo-Teruel, O.; Padilla, P. Dispersion Analysis of Periodic Structures in Anisotropic Media: Application to Liquid Crystals. *IEEE Trans. Antennas Propag.* **2021**. <https://doi.org/10.1109/TAP.2021.3137208>.
111. Weitsch, Y.; Eibert, T.F. Modal Series Expansion of Eigensolutions for Closed and Open Periodic Waveguides. *IEEE Trans. Antennas Propag.* **2012**, *60*, 5881–5889.
112. Giusti, F.; Mesa, F.; Chen, Q.; Valerio, G.; Quevedo-Teruel, O. Multimodal Transfer Matrix Method Applied to 3-D Periodic Structures. In Proceedings of the 2021 International Symposium on Antennas and Propagation (ISAP), Taipei, China, 25–28 January 2021; pp. 1–2.
113. Li, Z.Y.; Lin, L.L. Photonic band structures solved by a plane-wave-based transfer-matrix method. *Phys. Rev. E* **2003**, *67*, 046607. <https://doi.org/10.1103/PhysRevE.67.046607>.
114. Dassault Systèmes. CST Microwave Studio. Available online: <https://www.3ds.com/products-services/simulia/products/cst-studio-suite/solvers/> (accessed on 27 January 2022).
115. Ansys. Ansys HFSS. Available online: <https://www.ansys.com/products/electronics/ansys-hfss> (accessed on 27 January 2022).
116. Pendry, J.; Holden, A.; Robbins, D.; Stewart, W. Magnetism from conductors and enhanced nonlinear phenomena. *IEEE Trans. Microw. Theory Tech.* **1999**, *47*, 2075–2084. <https://doi.org/10.1109/22.798002>.
117. Freire, M.J.; Marques, R.; Jelinek, L. Experimental demonstration of a $\mu = -1$ metamaterial lens for magnetic resonance imaging. *Appl. Phys. Lett.* **2008**, *93*, 231108. <https://doi.org/10.1063/1.3043725>.
118. Algarín, J.M.; Freire, M.J.; Lapine, M. Ab initio experimental analysis of realistic resonant ring metamaterial lenses. In Proceedings of the 2010 IEEE Antennas and Propagation Society International Symposium, Toronto, Ontario, ON, Canada, 11–17 July 2010; pp. 1–4. <https://doi.org/10.1109/APS.2010.5561009>.
119. Baena, J.D.; Jelinek, L.; Marqués, R.; Silveirinha, M. Unified homogenization theory for magnetoinductive and electromagnetic waves in split-ring metamaterials. *Phys. Rev. A* **2008**, *78*, 013842. <https://doi.org/10.1103/PhysRevA.78.013842>.
120. Silveirinha, M.G. Artificial plasma formed by connected metallic wires at infrared frequencies. *Phys. Rev. B* **2009**, *79*, 035118. <https://doi.org/10.1103/PhysRevB.79.035118>.
121. Sievenpiper, D.F.; Sickmiller, M.E.; Yablonovitch, E. 3D Wire Mesh Photonic Crystals. *Phys. Rev. Lett.* **1996**, *76*, 2480–2483. <https://doi.org/10.1103/PhysRevLett.76.2480>.
122. Fietz, C.; Urzhumov, Y.; Shvets, G. Complex k band diagrams of 3D metamaterial/photonic crystals. *Opt. Express* **2011**, *19*, 19027–19041. <https://doi.org/10.1364/OE.19.019027>.
123. Belov, P.A.; Marqués, R.; Maslovski, S.I.; Nefedov, I.S.; Silveirinha, M.; Simovski, C.R.; Tretyakov, S.A. Strong spatial dispersion in wire media in the very large wavelength limit. *Phys. Rev. B* **2003**, *67*, 113103. <https://doi.org/10.1103/PhysRevB.67.113103>.
124. Sakhno, D.; Koreshin, E.; Belov, P.A. Longitudinal electromagnetic waves with extremely short wavelength. *Phys. Rev. B* **2021**, *104*, L100304.
125. Powell, A.W.; Mitchell-Thomas, R.C.; Zhang, S.; Cadman, D.A.; Hibbins, A.P.; Sambles, J.R. Dark Mode Excitation in Three-Dimensional Interlaced Metallic Meshes. *ACS Photonics* **2021**, *8*, 841–846.
126. Liang, B.; Bai, M. Subwavelength three-dimensional frequency selective surface based on surface wave tunneling. *Opt. Express* **2016**, *24*, 14697–14702. <https://doi.org/10.1364/OE.24.014697>.
127. Simovski, C.R.; Belov, P.A.; Atrashchenko, A.V.; Kivshar, Y.S. Wire Metamaterials: Physics and Applications. *Adv. Mater.* **2012**, *24*, 4229–4248.
128. Kushiya, Y.; Arima, T.; Uno, T. Experimental verification of spoof surface plasmons in wire metamaterials. *Opt. Express* **2012**, *20*, 18238–18247. <https://doi.org/10.1364/OE.20.018238>.
129. Gansel, J.K.; Thiel, M.; Rill, M.S.; Decker, M.; Bade, K.; Saile, V.; von Freymann, G.; Linden, S.; Wegener, M. Gold Helix Photonic Metamaterial as Broadband Circular Polarizer. *Science* **2009**, *325*, 1513–1515. <https://doi.org/10.1126/science.1177031>.
130. Faniayeu, I.; Asadchy, V.; Fanyayev, I. Polarization Control with Helical Metasurfaces. *Crystals* **2020**, *10*, 726. <https://doi.org/10.3390/cryst10090726>.
131. Wu, S.; Xu, S.; Zinenko, T.L.; Yachin, V.V.; Prosvirnin, S.L.; Tuz, V.R. 3D-printed chiral metasurface as a dichroic dual-band polarization converter. *Opt. Lett.* **2019**, *44*, 1056–1059. <https://doi.org/10.1364/OL.44.001056>.
132. Wu, S.; Yachin, V.V.; Shcherbinin, V.I.; Tuz, V.R. Chiral metasurfaces formed by 3D-printed square helices: A flexible tool to manipulate wave polarization. *J. Appl. Phys.* **2019**, *126*, 103101. <https://doi.org/10.1063/1.5114838>.
133. Fernandez-Corbaton, I.; Rockstuhl, C.; Ziemke, P.; Gumbsch, P.; Albiez, A.; Schwaiger, R.; Frenzel, T.; Kadac, M.; Wegener, M. New Twists of 3D Chiral Metamaterials. *Adv. Mater.* **2019**, *31*, 1807742. <https://doi.org/10.1002/adma.201807742>.

134. Ehrenberg, I.M.; Sarma, S.E.; Wu, B.I. A three-dimensional self-supporting low loss microwave lens with a negative refractive index. *J. Appl. Phys.* **2012**, *112*, 073114. <https://doi.org/10.1063/1.4757577>.
135. Sanz-Izquierdo, B.; Parker, E.A. 3-D Printing of Elements in Frequency Selective Arrays. *IEEE Trans. Antennas Propag.* **2014**, *62*, 6060–6066. <https://doi.org/10.1109/TAP.2014.2359470>.
136. Zhu, D.Z.; Gregory, M.D.; Werner, P.L.; Werner, D.H. Fabrication and Characterization of Multiband Polarization Independent 3-D-Printed Frequency Selective Structures With UltraWide Fields of View. *IEEE Trans. Antennas Propag.* **2018**, *66*, 6096–6105. <https://doi.org/10.1109/TAP.2018.2866507>.
137. Mittra, R.; Pelletti, C.; Arya, R.K.; Dong, T.; Bianconi, G. A general-purpose simulator for metamaterials with three-dimensional elements. In Proceedings of the 2013 International Symposium on Electromagnetic Theory, Hiroshima, Japan, 20–24 May 2013; pp. 78–80.
138. Pelletti, C.; Bianconi, G.; Mittra, R.; Shen, Z. Frequency selective surface with wideband quasi-elliptic bandpass response. *Electron. Lett.* **2013**, *49*, 1052–1053. <https://doi.org/10.1049/el.2013.2007>.
139. Pelletti, C.; Mittra, R.; Bianconi, G. Three-dimensional FSS elements with wide frequency and angular response. In Proceedings of the 2013 International Symposium on Electromagnetic Theory, Hiroshima, Japan, 20–24 May 2013; pp. 698–700.
140. Rashid, A.K.; Li, B.; Shen, Z. An overview of three-dimensional frequency-selective structures. *IEEE Antennas Propag. Mag.* **2014**, *56*, 43–67. <https://doi.org/10.1109/MAP.2014.6867682>.
141. Omar, A.A.; Shen, Z. Multiband High-Order Bandstop 3-D Frequency-Selective Structures. *IEEE Trans. Antennas Propag.* **2016**, *64*, 2217–2226. <https://doi.org/10.1109/TAP.2016.2546967>.
142. Omar, A.A.; Shen, Z.; Huang, H. Absorptive Frequency-Selective Reflection and Transmission Structures. *IEEE Trans. Antennas Propag.* **2017**, *65*, 6173–6178. <https://doi.org/10.1109/TAP.2017.2754463>.
143. Wang, W.; Cao, Q.; Zheng, Y. Bandstop Frequency-Selective Structures Based on Stepped-Impedance Loop Resonators: Design, Analysis, and Measurement. *IEEE Trans. Antennas Propag.* **2019**, *67*, 1053–1064. <https://doi.org/10.1109/TAP.2018.2880011>.
144. Omar, A.A.; Shen, Z. Thin 3-D Bandpass Frequency-Selective Structure Based on Folded Substrate for Conformal Radome Applications. *IEEE Trans. Antennas Propag.* **2019**, *67*, 282–290. <https://doi.org/10.1109/TAP.2018.2876706>.
145. Li, H.; Li, B.; Zhu, L. Wideband Bandpass Frequency-Selective Structures on Stacked Slotline Resonators: Proposal and Synthetic Design. *IEEE Trans. Antennas Propag.* **2020**, *68*, 7068–7078. <https://doi.org/10.1109/TAP.2020.2993312>.
146. Li, H.; Li, B.; Zhu, L. Wideband Linear-to-Circular Polarizer Based on Orthogonally Inserted Slot-Line Structures. *IEEE Antennas Wirel. Propag. Lett.* **2019**, *18*, 1169–1173. <https://doi.org/10.1109/LAWP.2019.2911550>.
147. Luo, G.Q.; Yu, W.; Yu, Y.; Zhang, X.H.; Shen, Z. A Three-Dimensional Design of Ultra-Wideband Microwave Absorbers. *IEEE Trans. Microw. Theory Tech.* **2020**, *68*, 4206–4215. <https://doi.org/10.1109/TMTT.2020.3011437>.
148. Omar, A.A.; Shen, Z. Double-Sided Parallel-Strip Line Resonator for Dual-Polarized 3-D Frequency-Selective Structure and Absorber. *IEEE Trans. Microw. Theory Tech.* **2017**, *65*, 3744–3752. <https://doi.org/10.1109/TMTT.2017.2700301>.
149. Zhou, L.; Shen, Z. 3-D Absorptive Energy-Selective Structures. *IEEE Trans. Antennas Propag.* **2021**, *69*, 5664–5672. <https://doi.org/10.1109/TAP.2021.3061097>.
150. Omar, A.A.; Shen, Z. Tunable Absorptive Frequency-Selective Transmission Structure. In Proceedings of the 2018 IEEE International Symposium on Antennas and Propagation USNC/URSI National Radio Science Meeting, Boston, MA, USA, 8–13 July 2018; pp. 2063–2064. <https://doi.org/10.1109/APUSNCURSINRSM.2018.8609167>.
151. Omar, A.A.; Kim, J.; Hong, W. A 3-D Lumped-Components-Free Absorptive Frequency-Selective Transmission Structure Featuring Very Wide Two-Sided Absorption Bandwidths. *IEEE Antennas Wirel. Propag. Lett.* **2020**, *19*, 761–765. <https://doi.org/10.1109/LAWP.2020.2979351>.
152. Yu, Y.; Luo, G.Q.; Liu, Q.; Yu, W.; Jin, H.; Liao, Z.; Shen, Z. 3D Band-Absorptive Frequency Selective Resorber: Concept and Analysis. *IEEE Access* **2019**, *7*, 2520–2528. <https://doi.org/10.1109/ACCESS.2018.2886967>.
153. Yu, W.; Luo, G.Q.; Yu, Y.; Liao, Z.; Jin, H.; Shen, Z. Broadband Band-Absorptive Frequency-Selective Resorber With a Hybrid 2-D and 3-D Structure. *IEEE Antennas Wirel. Propag. Lett.* **2019**, *18*, 1701–1705. <https://doi.org/10.1109/LAWP.2019.2928362>.
154. Yu, Y.; Shen, Z.; Deng, T.; Luo, G. 3-D Frequency-Selective Resorber With Wide Upper Absorption Band. *IEEE Trans. Antennas Propag.* **2017**, *65*, 4363–4367. <https://doi.org/10.1109/TAP.2017.2712812>.
155. Deng, T.; Yu, Y.; Chen, Z.N. A broadband 3D frequency selective resorber by using magnetic materials. In Proceedings of the 2017 International Conference on Electromagnetics in Advanced Applications (ICEAA), Verona, Italy, 11–15 September 2017; pp. 1731–1734. <https://doi.org/10.1109/ICEAA.2017.8065628>.
156. Wang, Y.; Wang, M.; Shen, Z.; Wu, W. 3-D Single- and Dual-Polarized Frequency-Selective Resorbers With Wide Absorption Bands Based on Stepped Impedance Resonator. *IEEE Access* **2021**, *9*, 22317–22327. <https://doi.org/10.1109/ACCESS.2021.3054461>.
157. Huang, H.; Shen, Z.; Hua, C. Ultra-Broadband 3-D Absorptive Frequency-Selective Transmission Structure Using Commercial Absorber. In Proceedings of the 2020 IEEE International Symposium on Antennas and Propagation and North American Radio Science Meeting, Montreal, QC, Canada, 5–10 July 2020; pp. 751–752. <https://doi.org/10.1109/IEEECONF35879.2020.9330467>.

158. Wang, Y.; Qi, S.S.; Shen, Z.; Wu, W. Ultrathin 3-D Frequency Selective Resorber With Wide Absorption Bands. *IEEE Trans. Antennas Propag.* **2020**, *68*, 4697–4705. <https://doi.org/10.1109/TAP.2020.2970116>.
159. Li, B.; Shen, Z. Wideband 3D Frequency Selective Resorber. *IEEE Trans. Antennas Propag.* **2014**, *62*, 6536–6541. <https://doi.org/10.1109/TAP.2014>
160. Ge, J.; Zhu, J.; Zhang, H.; Zhuang, W.; Tang, W. 3-D square coaxial waveguide FSS and equivalent circuit model. In Proceedings of the 2016 Progress in Electromagnetic Research Symposium (PIERS), Shanghai, China, 8–11 August 2016; pp. 1110–1114. <https://doi.org/10.1109/PIERS.2016.7734590>.
161. Tang, W.; Zhu, J.; Wang, C.; Ge, J.; Yu, Z.; Zhuang, W. Waveguide 3-D FSSs by 3-D printing technique. In Proceedings of the 2016 International Conference on Electromagnetics in Advanced Applications (ICEAA), Cairns, QLD, Australia, 19–23 September 2016; pp. 675–678. <https://doi.org/10.1109/ICEAA.2016.7731488>.
162. Zhu, J.; Ge, J.; Yao, J.; Hao, Z.; Tang, W. Dual-Band 3D Frequency Selective Surface Based on Square Coaxial Waveguide. In Proceedings of the 2018 International Conference on Microwave and Millimeter Wave Technology (ICMMT), Chengdu, China, 7–11 May 2018; pp. 1–3. <https://doi.org/10.1109/ICMMT.2018.8564006>.
163. Zhu, J.; Hao, Z.; Wang, C.; Yu, Z.; Huang, C.; Tang, W. Dual-Band 3-D Frequency Selective Surface With Multiple Transmission Zeros. *IEEE Antennas Wirel. Propag. Lett.* **2019**, *18*, 596–600. <https://doi.org/10.1109/LAWP.2019.2897369>.
164. Velasco, J.; Parellada-Serrano, I.; Molero, C. Fully Metallic Reflectarray for the Ku-Band Based on a 3D Architecture. *Electronics* **2021**, *10*. <https://doi.org/10.3390/electronics10212648>.
165. Sun, Y.X.; Wu, D.; Ren, J. Millimeter-Wave Dual-Polarized Dielectric Resonator Reflectarray Fabricated by 3D Printing With High Relative Permittivity Material. *IEEE Access* **2021**, *9*, 103795–103803. <https://doi.org/10.1109/ACCESS.2021.3098982>.
166. Bukhari, S.S.; Vardaxoglou, J.; Whittow, W. A Metasurfaces Review: Definitions and Applications. *Appl. Sci.* **2019**, *9*, 2727. <https://doi.org/10.3390/app9132727>.
167. Mei, P.; Zhang, S.; Pedersen, G.F. A Low-Cost, High-Efficiency and Full-Metal Reflectarray Antenna With Mechanically 2-D Beam-Steerable Capabilities for 5G Applications. *IEEE Trans. Antennas Propag.* **2020**, *68*, 6997–7006. <https://doi.org/10.1109/TAP.2020.2993077>.
168. Wang, X.; Cheng, Y.; Dong, Y. Millimeter-Wave Dual-Polarized Metal Transmitarray Antenna with Wide Gain Bandwidth. *IEEE Antennas Wirel. Propag. Lett.* **2022**. <https://doi.org/10.1109/LAWP.2021.3132172>.
169. Li, B.; Mei, C.Y.; Zhou, Y.; Lv, X. A 3-D-Printed Wideband Circularly Polarized Dielectric Reflectarray of Cross-Shaped Element. *IEEE Antennas Wirel. Propag. Lett.* **2020**, *19*, 1734–1738. <https://doi.org/10.1109/LAWP.2020.3015588>.
170. Yang, Y.; Wang, W.; Moitra, P.; Kravchenko, I.I.; Briggs, D.P.; Valentine, J. Dielectric Meta-Reflectarray for Broadband Linear Polarization Conversion and Optical Vortex Generation. *Nano Lett.* **2014**, *14*, 1394–1399. <https://doi.org/10.1021/nl4044482>.
171. Mei, P.; Zhang, S.; Pedersen, G.F. A Wideband 3-D Printed Reflectarray Antenna With Mechanically Reconfigurable Polarization. *IEEE Antennas Wirel. Propag. Lett.* **2020**, *19*, 1798–1802. <https://doi.org/10.1109/LAWP.2020.3018589>.
172. Cui, Y.; Nauroze, S.A.; Bahr, R.; Tentzeris, E.M. 3D Printed One-shot Deployable Flexible “Kirigami” Dielectric Reflectarray Antenna for mm-Wave Applications. In Proceedings of the 2020 IEEE/MTT-S International Microwave Symposium (IMS), Los Angeles, CA, USA, 4–6 August 2020; pp. 1164–1167. <https://doi.org/10.1109/IMS30576.2020.9224010>.
173. Liang, M.; Ng, W.R.; Chang, K.; Gbele, K.; Gehm, M.E.; Xin, H. A 3-D Luneburg Lens Antenna Fabricated by Polymer Jetting Rapid Prototyping. *IEEE Trans. Antennas Propag.* **2014**, *62*, 1799–1807. <https://doi.org/10.1109/TAP.2013.2297165>.
174. Wu, G.B.; Zeng, Y.S.; Chan, K.; Qu, S.W.; Chan, C. 3-D Printed Circularly Polarized Modified Fresnel Lens Operating at Terahertz Frequencies. *IEEE Trans. Antennas Propag.* **2019**, *67*, 4429–4437. <https://doi.org/10.1109/TAP.2019.2908110>.
175. Ishikawa, A.; Kato, T.; Takeyasu, N.; Fujimori, K.; Tsuruta, K. Selective electroless plating of 3D-printed plastic structures for three-dimensional microwave metamaterials. *Appl. Phys. Lett.* **2017**, *111*, 183102. <https://doi.org/10.1063/1.4986203>.
176. Sadeqi, A.; Rezaei Nejad, H.; Owyung, R.; Sonkusale, S. Three dimensional printing of metamaterial embedded geometrical optics (MEGO). *Microsyst. Nanoeng.* **2019**, *5*, 16. <https://doi.org/10.1038/s41378-019-0053-6>.
177. Kien, N.; Hong, I.P. Application of Metaheuristic Optimization Algorithm and 3D Printing Technique in 3D Bandpass Frequency Selective Structure. *J. Electr. Eng. Technol.* **2020**, *15*. <https://doi.org/10.1007/s42835-020-00370-4>.
178. Fernández Álvarez, H.; Cadman, D.; Goulas, A.; Gómez, M.; Engstrom, D.; Vardaxoglou, J.; Zhang, S. 3D conformal bandpass millimeter-wave frequency selective surface with improved fields of view. *Sci. Rep.* **2021**, *11*, 12846. <https://doi.org/10.1038/s41598-021-91218-y>.
179. Zhang, K.P.; Liao, Y.F.; Qiu, B.; Zheng, Y.K.; Yu, L.K.; He, G.H.; Chen, Q.N.; Sun, D.H. 3D Printed Embedded Metamaterials. *Small* **2021**, *17*, 2103262. <https://doi.org/10.1002/sml.202103262>.
180. Vásquez-Peralvo, J.A.; Tamayo-Domínguez, A.; Pérez-Palomino, G.; Fernández-González, J.M.; Wong, T. 3D Inductive Frequency Selective Structures Using Additive Manufacturing and Low-Cost Metallization. *Sensors* **2022**, *22*, 552. <https://doi.org/10.3390/s22020552>.
181. Harnois, M.; Himdi, M.; Yong, W.; Abdulrahim, S.; Tekkouk, K.; Cheval, N. An Improved Fabrication Technique for the 3-D Frequency Selective Surface based on Water Transfer Printing Technology. *Sci. Rep.* **2020**, *10*, 1714. <https://doi.org/10.1038/s41598-020-58657-5>.
182. Nauroze, S.A.; Novelino, L.S.; Tentzeris, M.M.; Paulino, G.H. Continuous-range tunable multilayer frequency-selective surfaces using origami and inkjet printing. *Proc. Natl. Acad. Sci. USA* **2018**, *115*, 13210–13215. <https://doi.org/10.1073/pnas.1812486115>.

183. Sung-Sil, C.; Sun-Hong, Y.; Ic-Pyo, Hong. Design of Three-Dimensional Frequency Selective Structure With Replaceable Unit Structures Using a 3-D Printing Technique. *IEEE Antennas Wirel. Propag. Lett.* **2018**, *17*, 2041–2045. <https://doi.org/10.1109/LAWP.2018.2871175>.
184. Burckel, D.B.; Wendt, J.R.; Ten Eyck, G.A.; Ellis, A.R.; Brener, I.; Sinclair, M.B. Fabrication of 3D Metamaterial Resonators Using Self-Aligned Membrane Projection Lithography. *Adv. Mater.* **2010**, *22*, 3171–3175. <https://doi.org/10.1002/adma.200904153>.
185. Xiong, X.; Xue, Z.H.; Meng, C.; Jiang, S.C.; Hu, Y.H.; Peng, R.W.; Wang, M. Polarization-dependent perfect absorbers/reflectors based on a three-dimensional metamaterial. *Phys. Rev. B* **2013**, *88*, 115105. <https://doi.org/10.1103/PhysRevB.88.115105>.
186. Pan, R.; Liu, Z.; Zhu, W.; Du, S.; Gu, C.; Li, J. Asymmetrical Chirality in 3D Bended Metasurface. *Adv. Funct. Mater.* **2021**, *31*, 2100689. <https://doi.org/10.1002/adfm.202100689>.
187. Taravati, S.; Eleftheriades, G.V. Generalized Space-Time-Periodic Diffraction Gratings: Theory and Applications. *Phys. Rev. Appl.* **2019**, *12*, 024026.
188. Tiukuvaara, V.; Smy, T.J.; Gupta, S. Floquet Analysis of Space-Time Modulated Metasurfaces With Lorentz Dispersion. *IEEE Trans. Antennas Propag.* **2021**, *69*, 7667–7678.
189. Huidobro, P.; Silveirinha, M.; Galiffi, E.; Pendry, J. Homogenization Theory of Space-Time Metamaterials. *Phys. Rev. Appl.* **2021**, *16*, 014044.
190. Caloz, C.; Deck-Léger, Z.L. Spacetime Metamaterials—Part I: General Concepts. *IEEE Trans. Antennas Propag.* **2020**, *68*, 1569–1582.
191. Caloz, C.; Deck-Léger, Z.L. Spacetime Metamaterials—Part II: Theory and Applications. *IEEE Trans. Antennas Propag.* **2020**, *68*, 1583–1598.
192. Taravati, S.; Eleftheriades, G.V. Microwave Space-Time-Modulated Metasurfaces. *ACS Photonics* **2022**.
193. Massa, A.; Marcantonio, D.; Chen, X.; Li, M.; Salucci, M. DNNs as Applied to Electromagnetics, Antennas, and Propagation—A Review. *IEEE Antennas Wirel. Propag. Lett.* **2019**, *18*, 2225–2229.
194. Fang, Z.; Zhan, J. Deep Physical Informed Neural Networks for Metamaterial Design. *IEEE Access* **2020**, *8*, 24506–24513.
195. Sagar, M.D.S.I.; Ouassal, H.; Omi, A.I.; Wisniewska, A.; Jalajamony, H.M.; Fernandez, R.E.; Sekhar, P.K. Application of Machine Learning in Electromagnetics: Mini-Review. *Electronics* **2021**, *10*, 2752.
196. Ramírez-Arroyo, A.; García, L.; Alex-Amor, A.; Valenzuela-Valdés, J.F. Artificial Intelligence and Dimensionality Reduction: Tools for approaching future communications. *arXiv* **2021**, arXiv:2112.10431.
197. Li, L.; et al. Machine-learning reprogrammable metasurface imager. *Nat. Commun.* **2019**, *10*, 1082.
198. Chahat, N.; Cook, B.; Estabrook, P. All-metal Dual Frequency RHCP High Gain Antenna for the Extreme Environments of a Potential Europa Lander. In Proceedings of the 2018 IEEE Indian Conference on Antennas and Propagation (InCAP), Krakow, Poland, 31 March–5 April 2018; pp. 1–3. <https://doi.org/10.1109/INCAP.2018.8770916>.
199. Matthaiou, M.; Yurduseven, O.; Ngo, H.Q.; Morales-Jimenez, D.; Cotton, S.L.; Fusco, V.F. The Road to 6G: Ten Physical Layer Challenges for Communications Engineers. *IEEE Commun. Mag.* **2021**, *59*, 64–69. <https://doi.org/10.1109/MCOM.001.2000208>.

-
200. Chen, R.; Long, W.X.; Wang, X.; Jiandong, L. Multi-Mode OAM Radio Waves: Generation, Angle of Arrival Estimation and Reception With UCAs. *IEEE Trans. Wirel. Commun.* **2020**, *19*, 6932–6947. <https://doi.org/10.1109/TWC.2020.3007026>.
 201. Zhang, B.; Zhan, Z.; Cao, Y.; Gulan, H.; Linnér, P.; Sun, J.; Zwick, T.; Zirath, H. Metallic 3-D Printed Antennas for Millimeter- and Submillimeter Wave Applications. *IEEE Trans. Terahertz Sci. Technol.* **2016**, *6*, 592–600. <https://doi.org/10.1109/TTHZ.2016.2562508>.